IEEE Transactions on Quantum Engineering

Received 15 April 2025; revised 8 December 2025; accepted 19 December 2025; date of publication 31 December 2025; date of current version 5 March 2026.

Digital Object Identifier 10.1109/TQE.2025.3649561

Quantum Error Correction for Second-Generation Quantum Repeaters

DAWEI JIAO[1], MAHDI BAYANIFAR[1] (Member, IEEE), ALEXEI ASHIKHMIN[2] (Fellow, IEEE), AND OLAV TIRKKONEN[1] (Fellow, IEEE)

[1]Department of Information and Communications Engineering, Aalto University, 00076 Aalto, Finland
[2]Nokia Bell Labs, Murray Hill, NJ 07974 USA

Corresponding author: Dawei Jiao (e-mail: dawei.jiao@aalto.fi).

This work was supported in part by Nokia Industrial Doctoral School in Quantum Technology and Business Finland under Grant 8264/31/2022.

ABSTRACT In this article, we consider second-generation (2G) quantum repeaters (QRs) for creating long-distance entanglement in quantum networks. Combining a distance-dependent depolarizing error model with the nonlocal Bell state purification procedure required by 2G QRs leads to an error model consisting of correlated and biased errors. To correct correlated errors, nonsymmetric Calderbank–Steane–Shor (CSS) codes with joint decoding between stations can be used. The dominating errors are biased, such that different repeater stations suffer from different types of errors. To mitigate this, different quantum codes can be used at the stations, optimized for the specific error model of the station. To comply with the 2G QR procedure, the codes used in neighboring stations must allow for the transversal implementation of nonlocal logical CNOT gates across the two stations or, alternatively, nonlocal CZ gates combined with logical Hadamard gates. We provide a complete characterization of pairs of CSS codes that allow CNOT or CZ transversality, and examine an explicit family of mirrored CSS codes allowing CZ transversality. We verify Hadamard gate transversality using our framework and show the importance of the logical qubit mapping matrix. Also, we conclude that using different QECCs does not lead to universal computation with the Clifford + T gate set. Finally, we study the entanglement generation rate (EGR) in 2G QRs with limited quantum memory, minimizing the number of intermediate stations for a given fidelity and EGR. By simulation, we observe that nonsymmetric and mirrored structure QECCs outperform the conventional approach of using symmetric CSS codes at the repeater stations.

INDEX TERMS Bell state purification, Calderbank–Steane–Shor (CSS) codes, key generation rate, quantum error correction, quantum repeater (QR), transversality.

I. INTRODUCTION

Quantum repeaters (QRs) are essential for building long-range quantum communication networks, including the quantum internet. As in classical communication systems, repeaters can be used to increase the communication rate in long-distance quantum communication [1].

The difference between classical and quantum communication is the no-cloning theorem, which states that it is impossible to create an identical copy of an unknown quantum state [2].

QRs overcome this challenge, extending the range of quantum communications without violating the no-cloning theorem. This makes them crucial for building efficient and secure long-distance quantum networks [1], [3], [4], [5]. At the present time, three generations of QRs have been considered, based on three different communication protocols. The first-generation QRs, known as *trusted node repeaters* [6], [7], use heralded entanglement purification and entanglement swapping to reduce erasure and operational errors [8], [9]. The main disadvantage of first-generation QRs is the requirement of long-range entangled quantum states, i.e., Bell states with sufficiently low physical error rate.

Second-generation (2G) QRs use QECCs, in addition to entanglement purification and swapping, for creating trusted long-range entanglement. With QECCs, we can tolerate more errors during transmission and increase the communication distance between stations while keeping the overall fidelity in reliable range [1], [10]. QECCs encode many

physical qubits into logical qubits and protect logical information with physical redundancy [11]. However, 2G QRs need classical communication between the stations, and the rate of end-to-end entanglement generation is limited due to the time-consuming Bell state purification process [12].

In third-generation QRs, the message is encoded by QECC and directly transmitted between stations [10]. In each station, the message is error corrected to recover from erasure errors and transmission errors. This generation depends mainly on QECCs, which require high-fidelity local quantum gates and large-scale QECCs.

In this article, we concentrate on 2G QRs, whose requirements are likely to be achievable in near-term quantum devices [13]. First, we formulate an explicit error model for 2G QRs, taking into account depolarizing errors in transmission and local two-qubit gate errors in each station during the Bell state purification. A similar channel was analyzed in [14], where the authors found a biased error model arising from the Bell state purification procedure. Second, we provide a detailed analysis of the nonlocal CNOT gate procedure, used to create entanglement between memory qubits in two stations. Considering the use of entanglement resources, local operations, measurement, and classical feedback, an error model of the nonlocal CNOT gate is provided. The resulting quantum channel has biased and correlated terms, with biased errors dominating. Here, we further show that nonsymmetric Calderbank–Steane–Shor (CSS) codes can be used to correct the correlated channel, and we propose a tailored code design to address the dominant biased errors.

In the 2G QR error model, different stations may suffer from different biased errors, which means that using different codes at the stations may lead to better performance. To comply with the nonlocal CNOT gate procedure, we need to keep the CNOT gate transversal for the pair of codes. Motivated by this, we provide sufficient and necessary conditions for CNOT gate transversality between different CSS codes. While similar cross-code operations have been explored in the context of lattice surgery and with the assistance of Pauli measurements [15], [16], [17], [18], these methods provide alternative approach for implementing logical operators across different QECCs. However, the additional resource overhead introduced by such approaches makes them less compatible with near-term 2G QR systems. In this work, rather than addressing universal fault-tolerant cross-code operations, we focus specifically on using transversal physical gates to implement logical operations within 2G QR architectures. Considering the fact that the transversal CZ gate with local operations leads to a nonlocal CNOT gate, we also provide sufficient conditions for achieving a transversal nonlocal CZ gate. We then design a family of mirrored structure codes for correcting different biased errors between neighboring stations and prove that these codes preserve the transversality of the logical CZ gate. It is known that a symmetric CSS code has Hadamard gate transversality. We verified this condition using our framework and show that the mapping matrix should fulfill specific conditions, which naturally arise from the commutation relation of the logical operations. We also provide an example of having both CZ and Hadamard gate transversalities using different codes at different stations and compare it with the mirrored structure code design. We also show that the mapping of logical to physical qubits in the pair of codes will affect transversality, and identify the conditions on the mapping matrices that allow transversality. We provide examples of pairs of CSS codes fulfilling either CNOT or CZ transversality. In addition, we discuss the possibility of universal computation via distinct QECCs. We conclude that, with this approach and using the Clifford + **T** gate, it is not possible to achieve transversality and universality simultaneously.

Finally, we consider the rate of end-to-end entanglement generation in a multihop 2G QR quantum communication scenario. In a situation with limited quantum memory, the time cost of generating purified Bell pairs, the distance-dependent depolarizing errors happening on the fiber, and the errors happening in the nonlocal CNOT gate leads to an intricate connection between the number of hops, the overall communication distance, the gate error rate, and the QECC used. We formulate an optimization problem for the length of a hop, given constraints on end-to-end fidelity and end-to-end entanglement generation rate (EGR).

With numerical simulation, we compare codes with CNOT and CZ transversality and show that, in a range of parameters, CZ-transversal codes achieve better fidelity. Through numerical evaluation, we show that given constraints on the end-to-end EGR and fidelity, the number of hops can be considerably reduced if mirrored structure codes are used instead of a pair of symmetric CSS codes. In particular for low gate error rate, we can reduce the number of hops to $1/3$ of the symmetric case.

The rest of this article is organized as follows. Preliminaries about QECCs, 2G QRs, and transversality can be found in Section II. Section III describes the detailed error model for 2G QRs. Based on this, two-QECC design is proposed in this section. In order to keep QR protocol fault-tolerant, conditions on CSS codes, which are CNOT or CZ transversal, are discussed in Section IV. The effect of logical qubit mapping and universality is also discussed in this section. In Section V, we analyze the rate of entanglement generation for 2G QRs and set the optimization conditions for minimizing the number of repeater stations. Numerical simulation results are shown in Section VI. Finally, Section VII concludes this article.

II. PRELIMINARIES

In this section, we provide the definition of the CSS codes and discuss the basic concepts of 2G QRs.

A. CSS CODES

CSS quantum error correction codes are a special case of stabilizer codes. They can be constructed based on two classical linear codes. Considering two linear codes $\mathcal{C}_1(n, k_1, d_1)$ and

$\mathcal{C}_2(n, k_2, d_2)$, such that $\mathcal{C}_2^{\perp} \subset \mathcal{C}_1$, a quantum $[[n, k, d]]$ CSS code $\mathcal{Q}_{12} \triangleq \text{CSS}(\mathcal{C}_1, \mathcal{C}_2)$ is defined as a linear subspace of dimension 2^k in $\mathbb{C}^{2^n}$ with the orthonormal basis [11]

$$|\boldsymbol{\psi}\rangle_L = \frac{1}{\sqrt{|\mathcal{C}_2^{\perp}|}} \sum_{\mathbf{y} \in \mathcal{C}_2^{\perp}} |\mathbf{x} + \mathbf{y}\rangle \tag{1}$$

where $\boldsymbol{\psi} \in \mathbb{F}_2^k$ and $\mathbf{x} \in \mathcal{C}_1$, a representative of the coset of $\mathcal{C}_2^{\perp}$ in the quotient group $\mathcal{C}_1/\mathcal{C}_2^{\perp}$ corresponding to $\boldsymbol{\psi}$. Note that $k = k_1 + k_2 - n$ and the code minimum distance is $d = \min(d_1, d_2^{\perp})$. In (1), we assume that the map between $\boldsymbol{\psi}$ and cosets of the group $\mathcal{C}_1/\mathcal{C}_2^{\perp}$ is linear, i.e., there exists an $k \times n$ binary logical qubit mapping matrix $\mathbf{A}$ such that $\mathbf{x} = \boldsymbol{\psi}\mathbf{A}$. Note that $|\boldsymbol{\psi}\rangle_L \in \mathbb{C}^{2^n}$ is the quantum state of n physical qubits corresponding to k logical qubits in the state $|\boldsymbol{\psi}\rangle \in \mathbb{C}^{2^k}$.

Consider the binary vectors $\mathbf{v} = [v_1, \ldots, v_n]$. The standard basis vector of $\mathbb{C}^N$ with $N = 2^n$ can be defined as $|\mathbf{v}\rangle = |v_1\rangle \otimes \ldots \otimes |v_n\rangle \in \mathbb{C}^N$, where $|0\rangle \triangleq [1, 0]^T$ and $|1\rangle \triangleq [0, 1]^T$ and $\otimes$ denotes the Kronecker (Tensor) product.

Pauli matrices for a single-qubit system are defined as

$$\mathbf{X} \triangleq \begin{bmatrix} 0 & 1 \\ 1 & 0 \end{bmatrix} \quad \mathbf{Z} \triangleq \begin{bmatrix} 1 & 0 \\ 0 & -1 \end{bmatrix} \quad \mathbf{Y} \triangleq \begin{bmatrix} 0 & -i \\ i & 0 \end{bmatrix} \tag{2}$$

where $i \triangleq \sqrt{-1}$. Pauli errors acting on n qubits have the form $\mathbf{E}(\mathbf{a}, \mathbf{b}) = i^{\mathbf{a}\mathbf{b}^T} \mathbf{D}(\mathbf{a}, \mathbf{b})$, where $\mathbf{D}(\mathbf{a}, \mathbf{b}) = \mathbf{X}^{a_1}\mathbf{Z}^{b_1} \otimes \ldots \otimes \mathbf{X}^{a_n}\mathbf{Z}^{b_n}$ and $\mathbf{a} = [a_1, \ldots, a_n]$, $\mathbf{b} = [b_1, \ldots, b_n]$ are binary vectors. We denote by γ the homomorphism defined by $\gamma(i^{\kappa}\mathbf{D}(\mathbf{a}, \mathbf{b})) = [\mathbf{a}^T, \mathbf{b}^T]$, $\kappa \in \{0, 1, 2, 3\}$.

A $\mathcal{Q}_{12} \triangleq \text{CSS}(\mathcal{C}_1, \mathcal{C}_2)$ code is an $[[n, k]]$ stabilizer code [11] whose $n - k$ generators correspond to binary vectors $\mathbf{g}_i$, $i = 1, \ldots, n-k$, in the form $[\mathbf{a}, \mathbf{0}]$ or $[\mathbf{0}, \mathbf{b}]$, $\mathbf{a}, \mathbf{b} \in \mathbb{F}_2^n$, and $\mathbf{0} \in \mathbb{F}_2^n$ is the all zero vector. Combining vectors $\mathbf{a}$ and $\mathbf{b}$, we obtain parity check matrices $\mathbf{H}(\mathcal{C}_2)$ and $\mathbf{H}(\mathcal{C}_1)$, respectively. Putting these matrices together, we obtain the matrix $\mathbf{G}^{\mathcal{Q}}$, which is the matrix of stabilizer generators of $\text{CSS}(\mathcal{C}_1, \mathcal{C}_2)$

$$\mathbf{G}^{\mathcal{Q}} = \left[\begin{array}{c|c} \mathbf{H}(\mathcal{C}_2) & \mathbf{0} \\ \hline \mathbf{0} & \mathbf{H}(\mathcal{C}_1) \end{array}\right] \tag{3}$$

The dimension of $\mathbf{G}^{\mathcal{Q}}$ is $(n - k) \times 2n$. Thus, with n qubits and $n - k$ generators, $\mathcal{Q}_{12}$ encodes k logical qubits. $\mathcal{C}_1$ and $\mathcal{C}_2$ are used to decode Pauli X and Z errors separately. The quantum code rate is defined as $R = k/n$. Increasing the code length n, while keeping R constant, we improve the code performance. However, the encoding and decoding complexities, and the number of operation errors, also grow with the code length n [19]. In a real physical system, we need to select a suitable code, based on the demand for logical fidelity and the accuracy of quantum operations.

Given $n - k$ stabilizer generators, we can define logical Pauli operators that are linearly independent and commute with all the generators. The Pauli operators can be represented as binary vectors. The $2n$ binary space can be decomposed into $2n$ independent basis vectors. In addition to the $n - k$ linear independent vectors given by the stabilizer, there exist $n + k$ linearly independent vectors. The logical Paulis also need to commute with the $n - k$ generators. We can thus find $n + k - (n - k) = 2k$ basis vectors, which give rise to the group $\mathbf{U}_L$ of logical Pauli operators with cardinality $|\mathbf{U}_L| = 4^k$. Thus, with k logical qubits, we have 4^k different logical Pauli operators.

B. SECOND-GENERATION QRS

Three generations of QRs exist based on different protocols, with 2G QRs likely to be realizable in the near future [4]. In contrast to the first generation, 2G QRs use QECCs to suppress the errors, which leads to a more efficient way to mitigate transmission errors in quantum communication. Third-generation repeaters provide a higher communication rate than 2G ones. However, they demand the transmission of many physical qubits to reduce the errors [12]. Second-generation repeaters, with the process of Bell state purification, have a lower rate, but they do not require large-scale QECCs. Thus, for near-future quantum registers with some hundreds of qubits, 2G QRs may be preferable.

In brief, the 2G QR protocol begins by establishing and purifying raw photonic Bell states between neighboring stations. These purified states are used to generate logical entanglements between qubits stored in the quantum memories at each station, enabling the correction of errors arising from local operations and memory decoherence. Finally, entanglement swapping is performed to establish end-to-end logical entanglements. More details are provided as follows.

1) The logical states $q_A = |+\cdots+\rangle_L$, where $|+\rangle = \frac{1}{\sqrt{2}}(|0\rangle + |1\rangle)$, and $q_B = |0\ldots0\rangle_L$ with k qubits are encoded into n physical qubits p_A and p_B in neighboring stations A and B.
2) Generate Bell pair qubits $b_1^1 b_2^1$ and $b_1^2 b_2^2$..., which are in state $\frac{1}{\sqrt{2}}(|00\rangle + |11\rangle)$ in station A and transmit b_2^t, $t = 1, 2, \ldots$, to station B through optic fiber.
3) Some of the transmitted qubits are lost on the channel. Heralded entanglement generation is used against erasure errors.
4) Among the qubits that station B has received successfully, Bell state purification is applied as follows [20]. CNOT gates are executed at A and B between qubits of two Bell states $b_1^t b_1^{t'}$ and $b_2^t b_2^{t'}$ with b_1^t and b_2^t as the control qubits, respectively. The target qubits are measured, with the outcome indicating whether purification succeeded. In this step, most Bell pairs are measured out and only a fraction of them will remain, with high fidelity.
5) A nonlocal CNOT gate is realized between p_A and p_B. CNOT gates are conducted at the stations from the physical qubits in memory to the Bell pair qubit, from p_A to b_1^t and b_2^t to p_B. The Bell pair qubits b_1^t b_2^t are measured. According to the measurement feedback, Pauli operators $\mathbf{Z}$ and $\mathbf{X}$ are applied on p_A and p_B separately. The nonlocal CNOT gate circuit is shown in Fig. 1.

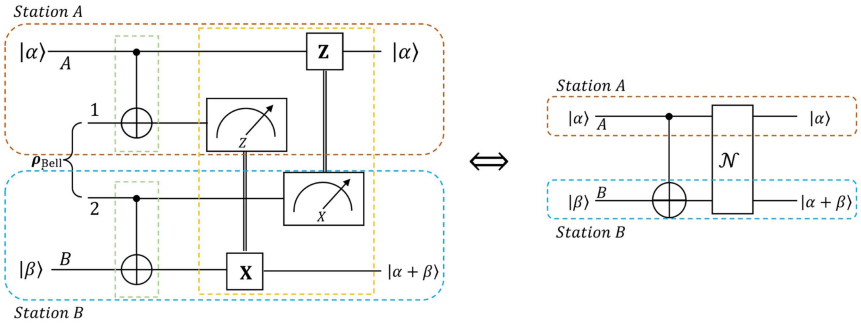

FIGURE 1. Nonlocal CNOT gate between stations *A* and *B* is applied using a Bell pair with two local CNOT gates. State $|\alpha\rangle$ and the first qubit of the Bell pair located in station *A*, while $|\beta\rangle$ and the second qubit of the Bell pair located in station *B*.

6) Transversal action of n nonlocal CNOT gates on n pairs of physical qubits p_A and p_B of step 5 leads to entanglement between logical qubits q_A and q_B. The resulting logical state between station A and B is $|00\rangle_L + |11\rangle_L$.
7) QECC is used in both stations to correct errors.
8) Entanglement swapping is performed at intermediate stations to achieve end-to-end entanglement [21]. Local CNOT gates are applied between code blocks related to two different hops. The measurements are performed simultaneously at all intermediate stations. The outcomes are sent to the outermost stations over the classical communication channel. These execute logical Pauli operators corresponding to the aggregate measurements to restore an end-to-end logical Bell state.

In 2G QRs, *QECCs with CNOT transversality* are used. This guarantees entanglement generation between q_A and q_B in step 6. Note that if a QECC with $k > 1$ is used, the transversal nonlocal CNOT gate would create entanglement between k pairs of logical qubits at station A and B.

The created end-to-end entanglement can be used for key generation or for quantum communication using quantum teleportation. Irrespective of the intended use, the essential parameters governing system performance are the end-to-end EGR and the fidelity of the created logical Bell state.

C. TRANSVERSALITY

QECCs encode many physical qubits into logical qubits and protect logical information from transmission and system operation noise by using redundancy. In 2G QRs systems, QECCs are used in each station to correct system errors. Logical entanglement is established between different code blocks; thus, it is important to keep the process fault-tolerant to prevent error propagation between different qubits. Transversal operators provide the easiest way to achieve fault-tolerant quantum circuits, i.e., preventing error propagation between different code blocks [22]. Transversality means that applying operations to the physical qubits in parallel leads to the same operations in the logical space. For an n-qubit error correction code, we can thus write the logical operator as

$$\mathbf{U}_L = \bigotimes_{i=1}^{n} \mathbf{U}_i \tag{4}$$

where $\mathbf{U}_i$ indicates the quantum operator $\mathbf{U}$ acting on qubit i.

Stabilizer codes are a family of widely investigated QECCs. In stabilizer codes, the information is stabilized by code generators, which are Pauli operators, into the stabilizer space [23]. CSS codes are a special case of stabilizer codes, wherein the generators are pure $\mathbf{X}$ and $\mathbf{Z}$ Pauli operators and the code is constructed by two classical linear codes [24]. The transversality of the CSS codes has been investigated in [25]. It was shown that all CSS codes have Pauli and CNOT gate transversality and that self-orthogonal CSS codes are also Hadamard and CZ transversal.

III. ERRORS AND ERROR CORRECTION FOR 2G QRS

In this section, we analyze the error channel originating from the 2G QR procedure and discuss two QECC designs that outperform conventional designs in this situation.

First, we consider two sources for errors: transmission errors and operation errors. Assuming that the 2G QR protocol completes within the coherence time of quantum memory, we neglect quantum memory errors. Then, we model how these basic errors propagate through key procedures: Bell state purification and nonlocal CNOT gate implementation. The fidelity relation between purified Bell state and initial input states through iteration of purification procedure has been well studied [26], [27]. As for nonlocal CNOT gate, we show that this procedure will lead to a special error model, which includes both biased and correlated errors. On the basis of the resulting error model, we show how to use different QECCs to tailor these different error models.

A. TRANSMISSION ERROR

The transmission of Bell pairs between neighboring stations through the optical fiber is susceptible to erasure and depolarizing errors that impact the photonic qubits. The crucial aspect of transmission errors is that the error probability depends on the distance between the stations. We model erasure

error probability as follows [28]:

$$e_0 = 1 - 10^{-\alpha L_0/10} \tag{5}$$

where L_0 is the distance between neighboring stations, and α is the attenuation coefficient, which depends on the medium that the qubits have been transmitted through. It is important to note that attenuation significantly influences the EGR. Given the erasure probability e_0, the transmitter needs on average $\frac{1}{1-e_0}$ attempts for a successful transmission of one photonic qubit.

In addition to erasures, we consider depolarizing errors, which model the errors resulting from the interaction of qubits with the environment. The depolarizing error rate also increases exponentially with the transmission distance. It can be modeled as [29]

$$\varepsilon_{de} = 1 - e^{-\beta L_0} \tag{6}$$

where β is the noise coefficient, which is a constant parameter depending on the quality of the medium.

The quantum transmission channel can thus be written as

$$\mathcal{N}_{tr}(\boldsymbol{\rho}) = (1 - \varepsilon_{de} - e_0)[\mathbf{I}](\boldsymbol{\rho}) + \frac{\varepsilon_{de}}{3}([\mathbf{X}]+[\mathbf{Y}]+[\mathbf{Z}])(\boldsymbol{\rho}). \tag{7}$$

Here, $[\mathbf{U}](\boldsymbol{\rho}) = \mathbf{U}(\boldsymbol{\rho})\mathbf{U}^\dagger$ represents the conjugate action of $\mathbf{U}$ on the density matrix $\boldsymbol{\rho}$. Note that with probability e_0, an erasure error happens. The qubit then vanishes on the channel and its density matrix at channel output is $\boldsymbol{\rho} = \mathbf{0}$.

B. OPERATION ERROR

We assume that all physical qubits and quantum operators are prone to depolarizing errors. Generally speaking, single-qubit gate errors and quantum memory errors are significantly less prevalent than two-qubit gate errors. For performance evaluation, we assume that these two types of errors are two orders of magnitude smaller than two-qubit gate errors [30]. Since the main two-qubit gate used in 2G QR is the CNOT gate, we focus on the CNOT gate error model. We use the depolarizing model for CNOT gate errors [27]

$$\mathcal{N}_{\text{CNOT}}(\boldsymbol{\rho}) = \left(1 - f_{\text{gate}}\right)[\mathbf{II}](\boldsymbol{\rho}) + \frac{f_{\text{gate}}}{16}\sum_{i,j=1}^{4}[\mathbf{P}_c^i\mathbf{P}_t^j](\boldsymbol{\rho}) \tag{8}$$

where $\mathbf{P}_c^i$ and $\mathbf{P}_t^j$ denote control and target qubit Pauli operators in the set $\{\mathbf{I}, \mathbf{X}, \mathbf{Y}, \mathbf{Z}\}$, respectively, and f_{gate} is the CNOT gate error rate.

C. ERROR MODEL FOR BELL STATE PURIFICATION

Upon reception of the noisy Bell state, we employ a Bell state purification procedure at both stations [26]. For K layers of purification, at least 2^K pairs of Bell states and $2^K - 1$ CNOT gates are needed. When more purification layers are used, the final Bell state achieves higher fidelity, as long as the initial fidelity is higher than 50% [28]. The Bell states go through a Pauli error channel, which leads to a Pauli error model for the Bell state

$$\boldsymbol{\rho}_{\text{Bell}} = f_0\boldsymbol{\rho}_{00} + f_1\boldsymbol{\rho}_{01} + f_2\boldsymbol{\rho}_{10} + f_3\boldsymbol{\rho}_{11} \tag{9}$$

where $f_0 = 1 - f_1 - f_2 - f_3$ is the fidelity, and

$$\boldsymbol{\rho}_{00} = \frac{1}{2}(|00\rangle + |11\rangle)(\langle 00| + \langle 11|)$$

$$\boldsymbol{\rho}_{01} = \frac{1}{2}(|01\rangle + |10\rangle)(\langle 01| + \langle 10|)$$

$$\boldsymbol{\rho}_{10} = \frac{1}{2}(|00\rangle - |11\rangle)(\langle 00| - \langle 11|)$$

$$\boldsymbol{\rho}_{11} = \frac{1}{2}(|01\rangle - |10\rangle)(\langle 01| - \langle 10|).$$

The ideal Bell state is $\boldsymbol{\rho}_{00}$, and f_1, f_2, and f_3 are the probability of $\boldsymbol{\rho}_{01}$, $\boldsymbol{\rho}_{10}$, and $\boldsymbol{\rho}_{11}$, respectively. If we use $\boldsymbol{\rho}_{00}$ as ideal state, other states can be written as a Pauli error acting on the ideal state

$$\boldsymbol{\rho}_{01} = \mathbf{X}\,\boldsymbol{\rho}_{00}\,\mathbf{X} \quad \boldsymbol{\rho}_{10} = \mathbf{Z}\,\boldsymbol{\rho}_{00}\,\mathbf{Z} \quad \boldsymbol{\rho}_{11} = \mathbf{ZX}\,\boldsymbol{\rho}_{00}\,\mathbf{XZ}.$$

Note that the two Pauli operators in $\mathbf{XZ}$ term can act on any of Bell pair qubits, since Bell state is the eigen state of $\mathbf{X_1X_2}$ and $\mathbf{Z_1Z_2}$ operations.

Since the transmitted photonic Bell pairs are corrupted by the distance-related depolarizing channel (7), the input states of first-level purification have error probabilities

$$f_1 = f_2 = f_3 = \varepsilon_{de}/3 \tag{10}$$

which are distance-related. After each level purification, new error probabilities can be calculated as follows [26]:

$$\begin{cases} f_0 = f_0'^2 + f_2'^2 \\ f_1 = 2f_0'f_1' \\ f_2 = 2f_2'f_3' \\ f_3 = f_1'^2 + f_3'^2 \end{cases} \tag{11}$$

Here, f_i and f_i' are probabilities of the purified and input states, respectively. Since the error probabilities should be small, such that $f_0 >> f_1 + f_2 + f_3$, for the purified state, we have $f_1 > f_2 + f_3$.

The purification success probability p_s is [26]

$$p_s = \left(f_0'+f_2'\right)^2 + \left(f_1'+f_3'\right)^2 = \left(1 - f_1' - f_3'\right)^2 + \left(f_1'+f_3'\right)^2 \tag{12}$$

where we used $\sum_i f_i' = 1$ for the second form. Only two types of Pauli errors affect the measurement outcome and the success probability. The biased error probabilities of purified Bell states were studied in [14], where a different Bell state purification procedure is used; this leads to a different, but also biased, error model for the output states.

D. ERROR MODEL FOR THE NONLOCAL CNOT GATE

In 2G QRs, logical entanglement between neighboring stations is established by transversal nonlocal CNOT gates. With the help of a shared purified Bell state, the nonlocal CNOT gate can be realized with high fidelity from a physical qubit in station A to the corresponding physical qubit in station B. The

resulting quantum channel arising from these operations was reported in [31]. Here, we provide the underlying analysis.

The purified Bell state as in (9) is used as input state to realize a nonlocal CNOT gate. The circuit of the nonlocal CNOT gate is shown in Fig. 1. This circuit is equivalent to a perfect CNOT gate with a noisy channel $\mathcal{N}$. If we neglect the local gate error, the parameters of $\mathcal{N}$ come from the purified state $\boldsymbol{\rho}_{\text{pur}}$.

First, we go through the situation with ideal input $\boldsymbol{\rho}_{00}$ to understand the procedure. The nonlocal state after the two CNOT gates before measurement can be described as

$$\begin{aligned}|\boldsymbol{\Psi}_{\text{ideal}}\rangle &= \boldsymbol{\Lambda}_{A,1}\boldsymbol{\Lambda}_{2,B}|\alpha\rangle_A \frac{1}{\sqrt{2}}(|00\rangle_{12}+|11\rangle_{12})|\beta\rangle_B \\ &= \alpha_0|000\beta\rangle + \alpha_0|011\beta'\rangle + \alpha_1|110\beta\rangle + \alpha_1|101\beta'\rangle \end{aligned} \tag{13}$$

where the subscript i indicates the ith qubit, $\boldsymbol{\Lambda}_{i,j}$ means CNOT gate from qubit i to j, with matrix

$$\boldsymbol{\Lambda} = \begin{bmatrix} 1 & 0 & 0 & 0 \\ 0 & 1 & 0 & 0 \\ 0 & 0 & 0 & 1 \\ 0 & 0 & 1 & 0 \end{bmatrix}$$

the first input state is $|\alpha\rangle = \alpha_0|0\rangle + \alpha_1|1\rangle$, and $|\beta'\rangle = \mathbf{X}|\beta\rangle$. Next, we conduct Z- and X-basis measurements on the second and third qubits. Each measurement has two outcomes with the same probability, which means that the final outcome is uniformly random. Using $\mathbf{M}_{Z,X}$ to represent the two measurement results, the state after the measurements are

$$\begin{cases} \mathbf{M}_{Z,X} = (+1,+1): & \alpha_0|00+\beta\rangle + \alpha_1|10+\beta'\rangle \\ \mathbf{M}_{Z,X} = (+1,-1): & \alpha_0|00-\beta\rangle - \alpha_1|10-\beta'\rangle \\ \mathbf{M}_{Z,X} = (-1,+1): & \alpha_0|01+\beta'\rangle + \alpha_1|11+\beta\rangle \\ \mathbf{M}_{Z,X} = (-1,-1): & \alpha_0|01-\beta'\rangle - \alpha_1|11-\beta'\rangle. \end{cases} \tag{14}$$

For $\mathbf{M}_{Z,X} = (+1,+1)$, the final state is the same as if a CNOT gate were executed; $\boldsymbol{\Lambda}_{\alpha\beta}|\alpha\rangle \otimes |\beta\rangle = \alpha_0|0\beta\rangle + \alpha_1|1\beta'\rangle$. For the other measurement outcomes, classical communication of the measurement results followed by single-qubit Pauli operators at different stations can recover the ideal state. For example, if we have $\mathbf{M}_{Z,X} = (+1,-1)$, then a Pauli $\mathbf{Z}$ operator at Station A will recover the state to ideal state, $\mathbf{Z}(\alpha_0|0\beta\rangle - \alpha_1|1\beta'\rangle) = \alpha_0|0\beta\rangle + \alpha_1|1\beta'\rangle$.

The action of the nonlocal CNOT gate on erroneous purified states in (9) can be analyzed in a similar manner. Due to the specific form of the noisy Bell state, only three types of Pauli errors have to be considered. For example, instead of an ideal Bell state, assume that $\boldsymbol{\rho}_{01}$ is the input of this circuit. Since the ideal Bell state $\boldsymbol{\rho}_{00}$ is an eigenstate of $\mathbf{XX}$ operator, this can arise in two ways—a Pauli $\mathbf{X}$ error happens either on the first or on the second qubit. First, assume that it happened on the first Bell state qubit, in station A. This error goes through the upper CNOT gate and affects the Z-basis measurement outcome. Because a recovery Pauli $\mathbf{X}$ operation is acting at Station B according to the measurement, the resulting outcome will have a Pauli $\mathbf{X}$ error on the physical qubit in station B. If an $\mathbf{X}$ error occur on the second Bell state qubit, after the lower CNOT gate, an $\mathbf{X}$ error propagates to the physical qubit in station B. The X-basis measurement on the second Bell pair qubit at Station B is robust to $\mathbf{X}$ errors, and will not be affected. This procedure thus also results in an $\mathbf{X}_B$ error.

We can similarly verify that a $\mathbf{Z}$ error, corresponding to $\boldsymbol{\rho}_{10}$ as the input state, will lead to a $\mathbf{Z}$ error in station A. When the first Bell state qubit has a $\mathbf{Z}$ error, it will propagate through the upper CNOT gate to the physical qubit in station A. A Z-basis measurement commutes with a $\mathbf{Z}$ error; thus, no error is propagated to station B, and the final state has a $\mathbf{Z}_A$ error. In the same way, we can see that a $\mathbf{Z}$ error on the second Bell state qubit will affect the X-basis measurement and also leads to a $\mathbf{Z}_A$ error.

Finally, the input state $\boldsymbol{\rho}_{11}$ arises when we have an $\mathbf{X}$ and a $\mathbf{Z}$ error on the qubits in the Bell pair. There are four equivalent alternatives for this. These result in the product error $\mathbf{Z}_A\mathbf{X}_B$ for the nonlocal CNOT gate. We can verify this by writing out the whole procedure. For the case when the two errors happen on the second qubit of the Bell pair, we have

$$\begin{aligned} &\boldsymbol{\Lambda}_{A,1}\boldsymbol{\Lambda}_{2,B}|\alpha\rangle_A \mathbf{Z}_1\mathbf{X}_1 \frac{1}{\sqrt{2}}(|00\rangle_{12}+|11\rangle_{12})|\beta\rangle_B \\ &= \mathbf{Z}_A\mathbf{Z}_1\mathbf{X}_1\boldsymbol{\Lambda}_{A,1}\boldsymbol{\Lambda}_{2,B}|\alpha\rangle_A \frac{1}{\sqrt{2}}(|00\rangle_{12}+|11\rangle_{12})|\beta\rangle_B \\ &= \mathbf{Z}_A\mathbf{Z}_1\mathbf{X}_2|\boldsymbol{\Psi}_{\text{ideal}}\rangle \end{aligned} \tag{15}$$

in terms of the ideal state in (13). Feedback is applied according to measurement outcomes, as in (14). When conducting measurements on the noisy state in (15), ancillary state qubits 1 and 2 are measured out. The Pauli $\mathbf{X}$ error on the first Bell pair qubit anticommutes with Z-basis measurement and flips the outcome. This leads to an additional $\mathbf{X}$ operator acting on $|\beta\rangle$. In the end, there is $\mathbf{Z}_A\mathbf{X}_B$ error on the final state.

As a consequence of the analysis above, the error channel $\mathcal{N}$ for a nonlocal CNOT gates becomes

$$\begin{aligned}\mathcal{N}(\boldsymbol{\rho}) = f_0[\mathbf{I}_A\mathbf{I}_B](\boldsymbol{\rho}) &+ f_1[\mathbf{Z}_A](\boldsymbol{\rho}) \\ &+ f_2[\mathbf{X}_B](\boldsymbol{\rho}) + f_3[\mathbf{Z}_A\mathbf{X}_B](\boldsymbol{\rho}). \end{aligned} \tag{16}$$

Here, hardware qubits in stations A and B are indicated by corresponding subscripts.

In this quantum channel, there are two characteristic parts. There are biased errors $[\mathbf{Z}_A]$ and $[\mathbf{X}_B]$—different types of Pauli errors occur in each station. In addition, there are correlated errors $[\mathbf{Z}_A\mathbf{X}_B]$, which occur in both stations simultaneously. For instance, the probability that the ith qubit in station A incurs a Pauli $\mathbf{Z}$ error is $f_1 + f_3$. When this happens, the conditional probability that the ith qubit in station B will experience a Pauli $\mathbf{X}$ error simultaneously is $f_3/(f_1+f_3)$.

IEEE Transactions on Quantum Engineering

Thus, in 2G QRs, in addition to gate errors, there exist biased and correlated errors introduced by Bell state purification that have to be taken into account. The biased and correlated errors grow as the distance between the neighboring stations increases and are significant when the gate error probability is sufficiently low.

From the recursion (11) of the purification errors, it follows that $f_1 > f_2, f_3$. Thus, the dominating term in the system is the biased error, specifically the biased $[\mathbf{Z}_A]$ happening in Station A. We can also apply single-qubit gates to the purified Bell pair, which can be described as (9), to exchange the values of f_1, f_2, and f_3, thereby adjusting the dominant error type. For example, applying the $\mathbf{S} \otimes \mathbf{S}^\dagger$ gate allows us to swap the values of f_1 and f_3

$$\mathbf{S} \otimes \mathbf{S}^\dagger \boldsymbol{\rho}_{\text{Bell}} \mathbf{S}^\dagger \otimes \mathbf{S} = f_0 \boldsymbol{\rho}_{00} + f_1 \boldsymbol{\rho}_{11} + f_2 \boldsymbol{\rho}_{10} + f_3 \boldsymbol{\rho}_{01} \tag{17}$$

where $\mathbf{S} = \begin{bmatrix} 1 & 0 \\ 0 & i \end{bmatrix}$, and $\mathbf{S}\mathbf{X}\mathbf{S}^\dagger = \mathbf{Y}$. Using this modified Bell pair as input Bell pair of nonlocal CNOT gate procedure, we can change error channel (16) into $\mathcal{N}'$

$$\begin{aligned} \mathcal{N}'(\boldsymbol{\rho}) = f_0[\mathbf{I}_A\mathbf{I}_B](\boldsymbol{\rho}) + f_3[\mathbf{Z}_A](\boldsymbol{\rho}) \\ + f_2[\mathbf{X}_B](\boldsymbol{\rho}) + f_1[\mathbf{Z}_A\mathbf{X}_B](\boldsymbol{\rho}) \end{aligned} \tag{18}$$

with $f_1 > f_2, f_3$. In this case, the dominating error is correlated error $[\mathbf{Z}_A\mathbf{X}_B]$. Based on these 2G QR error models, optimized QECC protocols can be designed.

We neglected the local gate error when deriving the nonlocal CNOT gate error model (16), which is independent of physical gate error rate f_{gate}. To complement the error model, we consider depolarizing errors for two-qubit gates as (8), resulting in

$$\begin{aligned} \mathcal{N}_O(\boldsymbol{\rho}) &= \mathcal{N}^2_{\text{CNOT}}(\mathcal{N}(\boldsymbol{\rho})) \\ &\approx (1 - 2f_{\text{gate}})\mathcal{N}(\boldsymbol{\rho}) + \frac{2f_{\text{gate}}}{16} \sum_{i,j=1}^{4} [\mathbf{P}_c^i \mathbf{P}_t^j] \mathcal{N}(\boldsymbol{\rho}) \end{aligned} \tag{19}$$

where $\mathcal{N}^2_{\text{CNOT}}$ stands for the error channel of two local CNOT gates used in the nonlocal CNOT gate circuit.

E. NONSYMMETRIC CSS CODES IN CORRELATED ERROR CHANNELS

It is important to note that in a 2G QR protocol, two blocks of logical qubits are mapped to physical qubits, one at station A and one at B. The objective is to create entanglement between stations A and B. Thus, in the encoding phase, there is no entanglement and the encoding has to be performed separately at stations A and B. However, decoding may be performed jointly at the stations, subject to an exchange of classical syndrome bits.

To achieve better performance, we need to design a proper QECC according to the dominant error in the system. As we discussed in the last section, the purified Bell state model (16) can be modified into the correlated-dominated error model (18), where $[\mathbf{Z}_A\mathbf{X}_B]$ is a dominated term. With such a channel, we can first assume $f_1 \gg f_2 + f_3$, concentrate an error model with only correlated errors, and neglect other errors

$$\mathcal{N}_{co} = (1 - f)[\mathbf{II}] + f[\mathbf{Z}^A\mathbf{X}^B] \tag{20}$$

where $\mathbf{Z}^A$ and $\mathbf{X}^B$ are Pauli operators acting on the qubit in stations A and B, respectively. This means that only $\mathbf{Z}$ errors occur in station A, and only $\mathbf{X}$ errors in station B, and these occur on the same physical qubits.

Now, we consider the situation where an $[[n, k, d]]$ stabilizer code $\mathcal{Q}$ with minimum distance $d = 2t + 1$ is used in stations A and B to encode the logical $|+\rangle$ and $|0\rangle$ states, respectively. We consider joint decoding at the two stations. That is, decoding is performed for the joint code $\mathcal{Q} \otimes \mathcal{Q}$.

For an error event e with weight $k > t$, there exists an error with weight $l \leq t$, which has the same syndrome as e. If we have a CSS code, a Pauli X-error event $e_{X1} = \prod_{i \in \mathcal{S}_1} \mathbf{X}_i$ on qubits in set $\mathcal{S}_1$ with $|\mathcal{S}_1| > t$ has the same syndrome as an error event $e_{X2} = \prod_{i \in \mathcal{S}_2} \mathbf{X}_i$ at positions $\mathcal{S}_2$ with $|\mathcal{S}_2| \leq t$.

The CSS code $\mathcal{Q}_{12}$ may be symmetric, with $\mathcal{C}_1 = \mathcal{C}_2 = \mathcal{C}$, or nonsymmetric. For a symmetric code, we have the same situation for Pauli $\mathbf{Z}$ errors as for $\mathbf{X}$ errors. Thus, $\mathbf{Z}$ error $e_{Z1} = \prod_{i \in \mathcal{S}_1} \mathbf{Z}_i$ has the same syndrome as $\mathbf{Z}$ error $e_{Z2} = \prod_{i \in \mathcal{S}_2} \mathbf{Z}_i$, and it cannot be corrected. As a consequence of this, we have the following proposition.

Proposition 1: Consider a nonsymmetric and a symmetric CSS code with the same minimum distance. They are used at stations A and B in quantum channel (20) with correlated $\mathbf{ZX}$ errors. With joint decoding at the stations, the nonsymmetric CSS code has smaller error probability than the symmetric one.

Proof: Consider Pauli error $e_{AB} = e^A_{X1} \otimes e^B_{Z1} = \prod_{i \in \mathcal{S}_1} \mathbf{X}^A_i \mathbf{Z}^B_i$, with $|\mathcal{S}_1| > t$ in neighboring stations A and B. With the error model (20), the probability of such error is $P(e_{AB}) = f^{w(e_{X1})}$, where $w(e^A_{X1})$ means the weight of Pauli error e^A_{X1}. According to the definition of a symmetric CSS code, there exists an error event $e_3 = e^A_{X2} \otimes e^B_{Z2} = \prod_{i \in \mathcal{S}_2} \mathbf{X}^A_i \mathbf{Z}^B_i$, with $|\mathcal{S}_2| \leq t$, which has the same syndrome as e_{AB}. The probability of this event is $P(e_3) = f^{w(e^A_{X2})}$. Since e^A_{X2} is a low weight error, $P(e_3) > P(e_{AB})$. In the error correction procedure, we select the error with the highest probability among the errors with the same syndrome. Accordingly, using symmetric CSS codes, we cannot recover e_{AB} errors. Thus, the decoding error probability will be $O(P(e_{AB}))$.

However, for the nonsymmetric CSS code, the error event with the same syndrome would be $e'_3 = e^A_{X2} \otimes e^B_{Z3} = \prod_{i \in \mathcal{S}_2} \prod_{j \in \mathcal{S}_3} \mathbf{X}^A_i \mathbf{Z}^B_j$ with $\mathcal{S}_2 \neq \mathcal{S}_3$. That is, $\mathbf{Z}$ and $\mathbf{X}$ errors would occur in different positions in stations A and B. In the error model (20), the probability of this type of error is $P(e'_3) = 0$. Thus, with a nonsymmetric CSS code, we can correct the e_{AB} error, and the decoding error rate would be lower than $O(P(e_{AB}))$, which is better than the symmetric CSS code. ■

F. DIFFERENT CSS CODES AT STATIONS A AND B FOR BIASED AND CORRELATED CHANNELS

Now we consider the more general error model (16), which contains both biased and correlated errors between two stations. According to this model, in station A, physical qubits are more prone to Pauli $\mathbf{Z}$ errors, while in station B, Pauli $\mathbf{X}$ errors are more prevalent. It is possible to use different codes at stations A and B, i.e., instead of the overall code $\mathcal{Q} \otimes \mathcal{Q}$, we may use $\mathcal{Q}_A \otimes \mathcal{Q}_B$. From the perspective of creating nonlocal entanglement, the overall QECC of interest is $\mathcal{Q}_A \otimes \mathcal{Q}_B$; there is no reason to limit oneself to $\mathcal{Q} \otimes \mathcal{Q}$.

For biased errors of type (16), it is possible to use a nonsymmetric code in station A that can correct more $\mathbf{Z}$ errors, and a different nonsymmetric code in station B that can correct more $\mathbf{X}$ errors. This approach may offer improved performance compared to using identical codes at both stations. For correcting biased errors, joint decoding is not strictly necessary because the biased errors are local errors. Although joint decoding can provide some additional benefit, the associated overhead in classical communication may negatively impact the EGR.

However, with this approach, the transversality of the logical CNOT gates needed to create logical entanglement between stations A and B cannot be guaranteed in general. Using transversal logical gates is the most common way to realize fault-tolerant quantum circuits. In the next section, we shall address the problem of designing different codes $\mathcal{Q}_A$ and $\mathcal{Q}_B$ for the two stations, such that transversality of two-qubit gates is fulfilled.

IV. TRANSVERSALITY WITH DIFFERENT CODES AT STATIONS A AND B

In this section, we study the restrictions for achieving transversality across two different codes with the same k and n. We assume that the QECCs used in stations A and B are CSS codes and investigate the transversality of logical CNOT and CZ gates between neighboring stations. We find a constructive method of creating a family of CZ transversal codes.

Note that here we only consider parallel logical CNOT/CZ. Each logical qubit of $\mathcal{Q}_A$ is paired with a logical qubit of $\mathcal{Q}_B$, and a transversal action of CNOT/CZ on the physical qubits of $\mathcal{Q}_A$ and $\mathcal{Q}_B$ realizes a CNOT/CZ acting on these pairs of logical qubits in parallel.

A. CNOT TRANSVERSALITY

Assume that we have two codes $\mathrm{CSS}(\mathcal{C}_1, \mathcal{C}_2)$ and $\mathrm{CSS}(\mathcal{C}_3, \mathcal{C}_4)$ in stations A and B, respectively. Our objective is to find sufficient conditions for having transversal CNOT. Let $\mathbf{G}_2^{\perp}$ and $\mathbf{G}_4^{\perp}$ be the generator matrices of $\mathcal{C}_2^{\perp}$ and $\mathcal{C}_4^{\perp}$, respectively. The generator matrices of $\mathcal{C}_1$ and $\mathcal{C}_3$ can then be written as

$$\mathbf{G}_1 = \begin{bmatrix} \mathbf{G}_2^{\perp} \\ \mathbf{A} \end{bmatrix} \qquad \mathbf{G}_3 = \begin{bmatrix} \mathbf{G}_4^{\perp} \\ \mathbf{B} \end{bmatrix} \tag{21}$$

where $\mathbf{A}$ and $\mathbf{B}$ are $k \times n$ binary matrices of rank k. These matrices map n-dimensional physical qubit space to k-dimensional logical space. For row space of mapping matrix $\mathbf{A}$, you can add any row belongs to $\mathbf{G}_2^{\perp}$ without changing the encoding states. But adding rows in $\mathbf{A}$ itself will change the mapping matrix and leads to the different encoding.

Let $\boldsymbol{\psi}^A, \boldsymbol{\psi}^B \in \mathbb{F}_2^k$. The code vectors of $\mathrm{CSS}(\mathcal{C}_1, \mathcal{C}_2)$ and $\mathrm{CSS}(\mathcal{C}_3, \mathcal{C}_4)$ corresponding to logical qubits in the states $|\boldsymbol{\psi}^A\rangle$ and $|\boldsymbol{\psi}^B\rangle$ are

$$|\boldsymbol{\psi}^A\rangle_L = \frac{1}{\sqrt{|\mathcal{C}_2^{\perp}|}} \sum_{\mathbf{y} \in \mathcal{C}_2^{\perp}} |\mathbf{x}^A + \mathbf{y}\rangle \tag{22}$$

$$|\boldsymbol{\psi}^B\rangle_L = \frac{1}{\sqrt{|\mathcal{C}_4^{\perp}|}} \sum_{\mathbf{z} \in \mathcal{C}_4^{\perp}} |\mathbf{x}^B + \mathbf{z}\rangle \tag{23}$$

where $\mathbf{x}^A = \boldsymbol{\psi}^A \mathbf{A}$ and $\mathbf{x}^B = \boldsymbol{\psi}^B \mathbf{B}$. We have the following theorem [32].

Theorem 1: Consider $\mathrm{CSS}(\mathcal{C}_1, \mathcal{C}_2)$ and $\mathrm{CSS}(\mathcal{C}_3, \mathcal{C}_4)$ codes in stations A and B, respectively, with generators given by (21). The logical CNOT gate between stations A and B is transversal iff

$$\mathcal{C}_2^{\perp} \subset \mathcal{C}_4^{\perp} \tag{24}$$

$$\mathcal{C}_1 / \mathcal{C}_2^{\perp} \cong \mathcal{C}_3 / \mathcal{C}_4^{\perp}. \tag{25}$$

Proof: For showing transversality, we need to show that applying CNOT gates to k pairs of logical qubits in the states $|\boldsymbol{\psi}^A\rangle_L$ and $|\boldsymbol{\psi}^B\rangle_L$ and then encoding the results into code vectors of $\mathrm{CSS}(\mathcal{C}_1, \mathcal{C}_2)$ and $\mathrm{CSS}(\mathcal{C}_3, \mathcal{C}_4)$ give the same result as first encoding logical qubits and then applying CNOT gates to n pairs of the physical qubits. If we first apply CNOT gates to logical qubits and then encoding into code vectors of $\mathrm{CSS}(\mathcal{C}_1, \mathcal{C}_2)$ and $\mathrm{CSS}(\mathcal{C}_3, \mathcal{C}_4)$, we get

$$\mathbf{\Lambda}_{AB}^{L} \left(|\boldsymbol{\psi}^A\rangle_L \otimes |\boldsymbol{\psi}^B\rangle_L \right) \triangleq |\boldsymbol{\psi}^A\rangle_L \otimes |\boldsymbol{\psi}^A \oplus \boldsymbol{\psi}^B\rangle_L . \tag{26}$$

Using (21) and (22) leads to

$$|\boldsymbol{\psi}^A \oplus \boldsymbol{\psi}^B\rangle_L = \frac{1}{\sqrt{|\mathcal{C}_4^{\perp}|}} \sum_{\mathbf{y} \in \mathcal{C}_4^{\perp}} |\left(\boldsymbol{\psi}^A + \boldsymbol{\psi}^B\right) \mathbf{B} + \mathbf{y}\rangle. \tag{27}$$

Next, by first encoding logical qubits in the states $|\boldsymbol{\psi}^A\rangle$ and $|\boldsymbol{\psi}^B\rangle$ and then applying CNOT gates to the n pairs of physical qubits, we get

$$\begin{aligned} &\mathbf{\Lambda}_{AB}^{P} \left(|\boldsymbol{\psi}^A\rangle_L \otimes |\boldsymbol{\psi}^B\rangle_L \right) \\ &= \frac{1}{\sqrt{|\mathcal{C}_2^{\perp}|\,|\mathcal{C}_4^{\perp}|}} \sum_{\mathbf{y} \in \mathcal{C}_2^{\perp}, \mathbf{z} \in \mathcal{C}_4^{\perp}} |\mathbf{x}^A + \mathbf{y}\rangle \otimes |\mathbf{x}^A + \mathbf{x}^B + \mathbf{y} + \mathbf{z}\rangle \\ &\overset{(a)}{=} \frac{1}{\sqrt{|\mathcal{C}_2^{\perp}|\,|\mathcal{C}_4^{\perp}|}} \sum_{\mathbf{y} \in \mathcal{C}_2^{\perp}, \mathbf{z}' \in \mathcal{C}_4^{\perp}} |\mathbf{x}^A + \mathbf{y}\rangle \otimes |\mathbf{x}^A + \mathbf{x}^B + \mathbf{z}'\rangle \end{aligned} \tag{28}$$

where (a), i.e., $\mathbf{y}$ is absorbed into the sum over $\mathbf{z}$, is true iff $\mathcal{C}_2^{\perp} \subset \mathcal{C}_4^{\perp}$ or equivalently $\mathcal{C}_4 \subset \mathcal{C}_2$.

For achieving the transversality, (26) has to be equal to (28) for all $\boldsymbol{\psi}^A$ and $\boldsymbol{\psi}^B$. This is possible if and only if $\mathbf{A} = \mathbf{B}$. Note that $\mathbf{A} = \mathbf{B}$ also means that $\mathcal{C}_1 / \mathcal{C}_2^{\perp} \cong \mathcal{C}_3 / \mathcal{C}_4^{\perp}$.

IEEE Transactions on Quantum Engineering

Note that we do not necessarily have $\mathcal{C}_1/\mathcal{C}_2^{\perp} = \mathcal{C}_3/\mathcal{C}_4^{\perp}$, since $\mathcal{C}_2^{\perp}$ can be smaller than $\mathcal{C}_4^{\perp}$, in which case the cosets will have different cardinality. The two quotient groups are still isomorphic. ■

If $\mathcal{C}_1 = \mathcal{C}_3$ and $\mathcal{C}_2 = \mathcal{C}_4$, the conditions of Theorem 1 are directly fulfilled. Thus, using the same CSS code at the stations results in CNOT transversality. This is in accordance with the fact that CSS codes are CNOT transversal [25].

Note that using (21) and the CNOT transversality conditions (24) and (25), we can rewrite the generators $\mathcal{C}_1$ and $\mathcal{C}_2$ allowing a transversal CNOT gate between stations A and B as

$$\mathbf{G}_1 = \begin{bmatrix} \mathbf{G}_2^{\perp} \\ \mathbf{A} \end{bmatrix} \qquad \mathbf{G}_3 = \begin{bmatrix} \mathbf{G}_2^{\perp} \\ \mathbf{D} \\ \mathbf{A} \end{bmatrix} \tag{29}$$

where $\mathbf{D}$ is the generator of $\mathcal{C}_4^{\perp}/\mathcal{C}_2^{\perp}$, which is a binary $(k_2 - k_4) \times n$ full rank matrix. It is worth to note that this structure implies that $\mathcal{C}_1 \subset \mathcal{C}_3$. Note that one could imagine from (29) that it is sufficient that $\mathcal{C}_1 \subset \mathcal{C}_3$ in order to have a transversal CNOT gate between the stations. This is, however, not correct. Consider, e.g., the case that $\mathcal{C}_1 = \mathcal{C}_4^{\perp} \subset \mathcal{C}_3$, i.e.,

$$\mathbf{G}_1 = \begin{bmatrix} \mathbf{G}_2^{\perp} \\ \mathbf{A} \end{bmatrix} \qquad \mathbf{G}_3 = \begin{bmatrix} \mathbf{G}_2^{\perp} \\ \mathbf{A} \\ \mathbf{D} \end{bmatrix}.$$

In this example, $\mathcal{C}_1 \subset \mathcal{C}_3$; however, this configuration does not satisfy (25). In the following, we provide an example that has a transversal CNOT gate between two stations.

Example 1: Transversal CNOT between two stations: Consider two CSS codes that map $k = 1$ logical qubits into $n = 7$ physical qubits: $\mathrm{CSS}(\mathcal{C}_1, \mathcal{C}_2)$ with $k_1 = 4$, $k_2 = 4$ and $\mathrm{CSS}(\mathcal{C}_3, \mathcal{C}_4)$ with $k_3 = 5$, $k_4 = 3$, having the following generators:

$$\mathbf{G}_1 = \begin{bmatrix} \mathbf{G}_2^{\perp} \\ \mathbf{A} \end{bmatrix} = \begin{bmatrix} 1\,1\,1\,1\,0\,0\,0 \\ 0\,1\,1\,1\,1\,0\,0 \\ 0\,0\,0\,1\,1\,1\,1 \\ \bar{1}\,\bar{1}\,\bar{1}\,\bar{1}\,\bar{1}\,\bar{1}\,0 \end{bmatrix}$$

$$\mathbf{G}_3 = \begin{bmatrix} \mathbf{G}_4^{\perp} \\ \mathbf{A} \end{bmatrix} = \begin{bmatrix} \mathbf{G}_2^{\perp} \\ \mathbf{D} \\ \mathbf{A} \end{bmatrix} = \begin{bmatrix} 1\,1\,1\,1\,0\,0\,0 \\ 0\,1\,1\,1\,1\,0\,0 \\ 0\,0\,0\,1\,1\,1\,1 \\ \bar{0}\,\bar{0}\,\bar{1}\,\bar{1}\,\bar{1}\,\bar{1}\,\bar{0} \\ \bar{1}\,\bar{1}\,\bar{1}\,\bar{1}\,\bar{1}\,\bar{1}\,0 \end{bmatrix}.$$

We then have a transversal nonlocal CNOT gate between stations A and B.

B. CZ TRANSVERSALITY

As a logical CNOT can be realized using a logical CZ across the two stations and local operations at the stations, it is possible to base a 2G QR protocol based on logical CZ transversality. As we shall see, this poses different requirements on the structure of the codes. We have the following theorem [32].

Theorem 2: Consider $\mathrm{CSS}(\mathcal{C}_1, \mathcal{C}_2)$ and $\mathrm{CSS}(\mathcal{C}_3, \mathcal{C}_4)$ codes in stations A and B, respectively, with generators given by (21). We have a transversal CZ gate between station A and B iff

$$\mathbf{x}^A \mathbf{z}^T + \mathbf{y}\left(\mathbf{x}^B + \mathbf{z}\right)^T = 0 \qquad \forall\, \mathbf{y} \in \mathcal{C}_2^{\perp},\ \mathbf{z} \in \mathcal{C}_4^{\perp} \tag{30}$$

$$\mathbf{A}\mathbf{B}^T = \mathbf{I}. \tag{31}$$

Proof: Using a similar approach used for the transversality of CNOT gate, first note that by applying logical CZ gate on the logical states, we get

$$\mathbf{CZ}_{AB}^{L} |\boldsymbol{\psi}^A\rangle_L \otimes |\boldsymbol{\psi}^B\rangle_L = (-1)^{\boldsymbol{\psi}^A (\boldsymbol{\psi}^B)^T} |\boldsymbol{\psi}^A\rangle_L \otimes |\boldsymbol{\psi}^B\rangle_L. \tag{32}$$

If we apply CZ to the n pairs of physical qubits, we get the following state:

$$\begin{aligned} &\mathbf{CZ}_{AB}^{P} |\boldsymbol{\psi}^A\rangle_L \otimes |\boldsymbol{\psi}^B\rangle_L \\ &= \alpha \sum_{\mathbf{y}\in\mathcal{C}_2^{\perp}, \mathbf{z}\in\mathcal{C}_4^{\perp}} (-1)^{(\mathbf{x}^A+\mathbf{y})(\mathbf{x}^B+\mathbf{z})^T} |\mathbf{x}^A + \mathbf{y}\rangle \otimes |\mathbf{x}^B + \mathbf{z}\rangle \\ &= \alpha\beta \sum_{\mathbf{y}\in\mathcal{C}_2^{\perp}, \mathbf{z}\in\mathcal{C}_4^{\perp}} (-1)^{\mathbf{x}^A \mathbf{z}^T + \mathbf{y}(\mathbf{x}^B+\mathbf{z})^T} |\mathbf{x}^A + \mathbf{y}\rangle \otimes |\mathbf{x}^B + \mathbf{z}\rangle \end{aligned} \tag{33}$$

where $\alpha = 1/\sqrt{|\mathcal{C}_2^{\perp}||\mathcal{C}_4^{\perp}|}$ and $\beta = (-1)^{\mathbf{x}^A(\mathbf{x}^B)^T}$. For having a transversal CZ gate, (32) should be equal to (33). According to the definition of the logical qubits, it is clear that (30) should be satisfied. Also, considering that $\mathbf{x}^A = \boldsymbol{\psi}^A\mathbf{A}$ and $\mathbf{x}^B = \boldsymbol{\psi}^B\mathbf{B}$, then $\beta = (-1)^{\boldsymbol{\psi}^A \mathbf{A}\mathbf{B}^T (\boldsymbol{\psi}^B)^T}$. Considering (32), we need to have $\beta = (-1)^{\boldsymbol{\psi}^A(\boldsymbol{\psi}^B)^T}$, which means that we have $\mathbf{A}\mathbf{B}^T = \mathbf{I}$. This completes the proof. ■

Corollary 1: Consider CSS codes at stations A and B as in Theorem 2. A sufficient condition for having a transversal CZ gate between the stations is [32]

$$\mathcal{C}_1/\mathcal{C}_2^{\perp} \cong \mathcal{A}_1, \quad \mathcal{C}_3 \subseteq \mathcal{C}_2, \quad \mathbf{A}\mathbf{B}^T = \mathbf{I} \tag{34}$$

or

$$\mathcal{C}_1 \subseteq \mathcal{C}_4, \quad \mathcal{C}_3/\mathcal{C}_4^{\perp} \cong \mathcal{B}_1, \quad \mathbf{A}\mathbf{B}^T = \mathbf{I} \tag{35}$$

where $\mathcal{A}_1 \subset \mathcal{C}_4$ and $\mathcal{B}_1 \subset \mathcal{C}_2$ are sets of vectors $\mathbf{c} \in \mathbb{F}_2^n$.

Proof: We note that for satisfying (30), one of the following conditions is sufficient.

1) $\mathbf{x}^A\mathbf{z}^T = 0$ and $\mathbf{y}(\mathbf{x}^B + \mathbf{z})^T = 0$: this happens when $\mathcal{C}_1/\mathcal{C}_2^{\perp} \cong \mathcal{A}_1 \subset \mathcal{C}_4$ and $\mathcal{C}_3 \subset \mathcal{C}_2$.
2) $\mathbf{x}^A\mathbf{z}^T = 1$ and $\mathbf{y}(\mathbf{x}^B + \mathbf{z})^T = 1$: this cannot happen since $\mathbf{z}$ belongs to a linear code.
3) $(\mathbf{x}^A + \mathbf{y})\mathbf{z}^T = 0$ and $\mathbf{y}(\mathbf{x}^B)^T = 0$: this happens when $\mathcal{C}_1 \subset \mathcal{C}_4$ and $\mathcal{C}_3/\mathcal{C}_4^{\perp} \subset \mathcal{C}_2$.
4) $(\mathbf{x}^A + \mathbf{y})\mathbf{z}^T = 1$ and $\mathbf{y}(\mathbf{x}^B)^T = 1$: this cannot happen since $\mathbf{z}$ belongs to a linear code.

Noting that $\mathbf{A}\mathbf{B}^T = \mathbf{I}$ should be satisfied as well completes the proof. ■

C. MIRRORED STRUCTURE FOR CZ TRANSVERSALITY

An example of CZ transversality between two stations is provided by mirrored nonsymmetric CSS codes, defined as follows. Consider two classical linear codes $\mathcal{C}_1$ and $\mathcal{C}_2$ with minimum distances d_1 and d_2, respectively. For constructing the nonsymmetric CSS code, $\text{CSS}(\mathcal{C}_1, \mathcal{C}_2)$, we assume that $\mathcal{C}_2^\perp \subset \mathcal{C}_1$ and $d_1 > d_2$. We use $\mathcal{C}_1$ and $\mathcal{C}_2$ to correct Pauli $\mathbf{Z}$ and $\mathbf{X}$ errors, respectively.

We then construct another code $\text{CSS}(\mathcal{C}_3, \mathcal{C}_4)$ such that $\mathcal{C}_4^\perp \subset \mathcal{C}_3$ with $\mathcal{C}_3 = \mathcal{C}_2$ and $\mathcal{C}_4 = \mathcal{C}_1$. Therefore, in this code, $\mathcal{C}_2$ and $\mathcal{C}_1$ are used for correcting $\mathbf{Z}$ and $\mathbf{X}$ errors, respectively. The generator matrices of mirrored CSS codes can be written as

$$\begin{bmatrix} \mathbf{G_2^\perp} & \mathbf{0} \\ \mathbf{0} & \mathbf{G_1^\perp} \end{bmatrix} \begin{bmatrix} \mathbf{G_4^\perp} & \mathbf{0} \\ \mathbf{0} & \mathbf{G_3^\perp} \end{bmatrix} = \begin{bmatrix} \mathbf{G_1^\perp} & \mathbf{0} \\ \mathbf{0} & \mathbf{G_2^\perp} \end{bmatrix} \tag{36}$$

where $\mathbf{0}$ is the all-zero matrix.

Example 2: Consider a pair of mirrored CSS codes $\text{CSS}(\mathcal{C}_1, \mathcal{C}_2)$ and $\text{CSS}(\mathcal{C}_3, \mathcal{C}_4)$, between stations A and B with generator matrices [32]

$$\mathbf{G_1^\perp} = \begin{bmatrix} 1 & 1 & 0 & 0 & 1 & 0 & 0 \\ 1 & 1 & 1 & 0 & 0 & 1 & 0 \\ 1 & 1 & 1 & 0 & 0 & 0 & 1 \end{bmatrix}$$

$$\mathbf{G_2^\perp} = \begin{bmatrix} 1 & 1 & 0 & 0 & 0 & 0 & 0 \\ 0 & 1 & 0 & 1 & 1 & 1 & 1 \end{bmatrix}.$$

These codes are CZ transversal according to Corollary 1. After simple manipulations, we find that

$$\mathbf{G}_4 = \mathbf{G}_1 = \begin{bmatrix} \mathbf{G_2^\perp} \\ \mathbf{A} \end{bmatrix} = \begin{bmatrix} 1\,1\,0\,0\,0\,0\,0 \\ 0\,1\,0\,1\,1\,1\,1 \\ \bar{0}\,\bar{0}\,\bar{1}\,\bar{1}\,\bar{0}\,\bar{1}\,\bar{1} \\ 1\,0\,1\,1\,1\,0\,0 \end{bmatrix}$$

$$\mathbf{G}_2 = \mathbf{G}_3 = \begin{bmatrix} \mathbf{G_4^\perp} \\ \mathbf{B} \end{bmatrix} = \begin{bmatrix} 0\,0\,0\,0\,1\,1\,0 \\ 0\,0\,0\,0\,1\,0\,1 \\ 1\,1\,0\,0\,0\,1\,0 \\ \bar{0}\,\bar{1}\,\bar{1}\,\bar{1}\,\bar{0}\,\bar{0}\,\bar{1} \\ 0\,1\,1\,0\,0\,0\,1 \end{bmatrix}.$$

Now, $\mathcal{C}_1/\mathcal{C}_2^\perp \subset \mathcal{C}_4$, $\mathcal{C}_3 = \mathcal{C}_2$, and $\mathbf{AB}^T = I_2$. Thus, the conditions (34) are satisfied, and this pair of mirrored CSS codes is indeed CZ transversal.

It is straight forward to see that any CSS codes with generators (36) satisfy the first two conditions of (34). By analyzing the third condition, we have the following corollary.

Corollary 2: Consider a pair of mirrored CSS codes with $\mathcal{C}_1 = \mathcal{C}_4$ and $\mathcal{C}_2 = \mathcal{C}_3$. Any such pair can be transformed to satisfy the sufficient conditions for CZ transversality by row-wise operations on matrix $\mathbf{A}$ or $\mathbf{B}$.

Proof: In the mirrored structure, the component code generators of (21) can be written as

$$\mathbf{G}_1 = \begin{bmatrix} \mathbf{G_3^\perp} \\ \mathbf{A} \end{bmatrix} \qquad \mathbf{G}_3 = \begin{bmatrix} \mathbf{G_1^\perp} \\ \mathbf{B} \end{bmatrix}. \tag{37}$$

From the mirrored structure, it directly follows that the first condition of (34) is fulfilled, as $\mathcal{C}_1/\mathcal{C}_2^\perp \subset \mathcal{C}_1 = \mathcal{C}_4$, while the second condition is fulfilled by definition. To prove that mirrored structure codes are CZ transversal, we need to show that $\mathbf{AB}^T = \mathbf{I}$. In general, $\text{rank}(\mathbf{AB}^T) \leq \min(\text{rank}(\mathbf{A}), \text{rank}(\mathbf{B}))$. However, due to the structure in (37), $\mathbf{AB}^T$ is a full rank matrix.

To prove this, assume that it is not full rank. The (i, j)th entry of $\mathbf{AB}^T$ is $\mathbf{a}_i\mathbf{b}_j^T$, where $\mathbf{a}_i$ and $\mathbf{b}_j$ are ith and jth row of $\mathbf{A}$ and $\mathbf{B}$, respectively. If $\mathbf{AB}^T$ is not full rank, its columns are dependent; there exists a binary vector $\mathbf{x} = (x_1, x_2, \ldots, x_n)$ such that $\sum_i x_i\,\mathbf{a}_i\mathbf{B}^T = \mathbf{0}$. If we define $\mathbf{a}' = \Sigma_i x_i \mathbf{a}_i$, we then have $\mathbf{a}' \in \mathbf{B}^\perp$. According to (36), for mirrored CSS codes, code spaces and their duals are related as

$$\mathbf{G_1} = \begin{bmatrix} \mathbf{G_3^\perp} \\ \mathbf{A} \end{bmatrix} \qquad \mathbf{G_3} = \begin{bmatrix} \mathbf{G_1^\perp} \\ \mathbf{B} \end{bmatrix}.$$

For a rank-deficient $\mathbf{AB}^T$, we thus would have $\mathbf{G}_3^\perp = \mathbf{G}_1 \cap \mathbf{B}^\perp$, as $\mathbf{a}'$ is a linear combination of $\mathbf{a}_i \in \mathbf{A} \subset \mathbf{G_1}$. Thus, $\mathbf{a}' \in \mathbf{G}_3^\perp$, which means that $\mathbf{G}_1$ is not full rank, which is a contradiction. Thus, $\mathbf{AB}^T$ has to be full rank. From this, it follows that using Gaussian elimination, we can find a $\mathbf{W}$ such that $\mathbf{WAB}^T = \mathbf{A}'\mathbf{B}^T = \mathbf{I}$. This means that by selecting a proper $\mathbf{A}$ in station A, CZ transversality is achievable. ■

D. HADAMARD GATE TRANSVERSALITY

In 2G QRs, we need logical CNOT gates to establish logical entanglement. A CZ gate can be converted to a CNOT gate with two additional Hadamard gates.

In the literature [25], the Hadamard gate transversality is proved via stabilizer generator algebra. For a $\text{CSS}(\mathcal{C}_1, \mathcal{C}_2)$ code with generators given by (21), the code has a transversal Hadamard gate iff $\mathcal{C}_1 = \mathcal{C}_2$. Here, we verify Hadamard gate transversality in our framework in order to find out whether the encoding matrix has an effect on Hadamard gate transversality.

The action of m parallel Hadamard gates on m-qubit state $|\mathbf{a}\rangle$ can be expressed as

$$\mathbf{H}^{\otimes m}|\mathbf{a}\rangle = \frac{1}{\sqrt{2^m}} \sum_{\mathbf{b}\in\mathbb{F}_2^m} (-1)^{\mathbf{ab}^T} |\mathbf{b}\rangle. \tag{38}$$

For the $[[n, k, d]]$ CSS code with the generator matrix as (3), it has Hadamard gate transversality, when it satisfies $\mathbf{H}_L^{\otimes k}|\boldsymbol{\psi}\rangle_L = \mathbf{H}^{\otimes n}|\boldsymbol{\psi}\rangle$, where $\mathbf{H}_L$ indicates logical Hadamard gate, and $|\boldsymbol{\psi}\rangle$ denotes the corresponding n qubits physical state. We can write the logical parallel Hadamard gate acting on the logical state as

$$\begin{aligned} \mathbf{H}_L^k|\boldsymbol{\psi}\rangle_L &= \frac{1}{\sqrt{2^k}} \sum_{\boldsymbol{\psi}_b\in\mathbb{F}_2^k} (-1)^{\boldsymbol{\psi}\boldsymbol{\psi}_b^T} |\boldsymbol{\psi}_b\rangle_L \\ &= \frac{1}{\sqrt{2^k}\sqrt{|\mathcal{C}_2^\perp|}} \sum_{\boldsymbol{\psi}_b\in\mathbb{F}_2^k} \sum_{\mathbf{y}\in\mathcal{C}_2^\perp} (-1)^{\boldsymbol{\psi}\boldsymbol{\psi}_b^T} |\mathbf{A}\boldsymbol{\psi}_b + \mathbf{y}\rangle \end{aligned} \tag{39}$$

IEEE Transactions on Quantum Engineering

where $\mathbf{A}$ is the mapping matrix in (21). Since $\mathbf{A} \in \mathcal{C}_1/\mathcal{C}_2^\perp$ and $\boldsymbol{\psi}_b$ is summed over $\mathbb{F}_2^k$, the double summation over $\boldsymbol{\psi}_b$ and $\mathbf{y}$ consists of all the codewords in $\mathcal{C}_1$.

We also can write n parallel physical Hadamard gates acting on the logical state as

$$\begin{aligned}\mathbf{H}^{\otimes n}|\boldsymbol{\psi}\rangle_L &= \frac{1}{\sqrt{|\mathcal{C}_2^\perp|}}\sum_{\mathbf{z}\in\mathcal{C}_2^\perp}\mathbf{H}^{\otimes n}|\mathbf{x}+\mathbf{z}\rangle \\ &= \frac{1}{\sqrt{2^n}\sqrt{|\mathcal{C}_2^\perp|}}\sum_{\mathbf{z}\in\mathcal{C}_2^\perp}\sum_{\mathbf{x}_b'\in\mathbb{F}_2^n}(-1)^{(\mathbf{x}+\mathbf{z})\mathbf{x}_b'^T}|\mathbf{x}_b'\rangle \\ &= \frac{\sqrt{|\mathcal{C}_2^\perp|}}{\sqrt{2^n}}\sum_{\mathbf{x}_b'\in\mathcal{C}_2}(-1)^{\boldsymbol{\psi}\mathbf{A}\mathbf{x}_b'^T}|\mathbf{x}_b'\rangle. \end{aligned} \tag{40}$$

If we want (39) to be equal to (40), it is a necessary condition that $\mathcal{C}_2 = \mathcal{C}_1$; then, these two equations contain the same physical states.

Then, we can check the normalize parameter of two equations; since we assume an $[[n, k, d]]$ CSS code with $\mathcal{C}_2 = \mathcal{C}_1$, we can get that the classical code has parameter $[n, k']$ as $2k' - n = k$. $\mathcal{C}_2^\perp$ has cardinality $|\mathcal{C}_2^\perp| = 2^{\frac{n-k}{2}}$. We can rewrite the parameter of (40) as

$$\frac{\sqrt{|\mathcal{C}_2^\perp|}}{\sqrt{2^n}} = \sqrt{2^{\frac{n-k}{2}-n}} = \frac{1}{\sqrt{2^{\frac{n+k}{2}}}} = \frac{1}{\sqrt{|\mathcal{C}_2^\perp|}\sqrt{2^k}}.$$

We get the same normalize parameter for both equations.

Finally, for the equality to hold, the sign for each state should coincide, up to a possible global phase. To address the same physical state in both equations, we have $\mathbf{x}_b' = \mathbf{A}\boldsymbol{\psi}_b + \mathbf{y}$. We can rewrite the phase factor in (40) as

$$(-1)^{\boldsymbol{\psi}\mathbf{A}\mathbf{x}_b'^T} = (-1)^{\boldsymbol{\psi}\mathbf{A}\mathbf{A}^T\boldsymbol{\psi}_b^T + \boldsymbol{\psi}\mathbf{A}\mathbf{y}^T}.$$

Since $\boldsymbol{\psi}\mathbf{A} \in \mathcal{C}_1$, $\mathbf{y} \in \mathcal{C}_2^\perp$, and $\mathcal{C}_1 = \mathcal{C}_2$, we have $\boldsymbol{\psi}\mathbf{A}\mathbf{y}^T = \mathbf{0}$. The only possibility for (39) to be equal to (40) up to a global phase is, thus, $\mathbf{A}\mathbf{A}^T = \mathbf{I}$. Note that while this seems an additional condition for Hadamard transversality, it can be readily understood from the role of the mapping matrix $\mathbf{A}$. We shall see in Section IV-E that the rows of $\mathbf{A}$ represent logical $\mathbf{X}$ operators of the quantum code. The condition $\mathbf{A}\mathbf{A}^T = \mathbf{I}$ thus naturally holds for symmetric CSS codes as a consequence of the commutation rules of logical operators.

For use in 2G QRs, to create a nonlocal CNOT gate, we can combine a transversal Hadamard gate with a transversal nonlocal CZ gate to achieve a transversal CNOT gate in a specific equation. Recall that for CZ transversality, the codes need to satisfy (34) or (35), as well as the transversal Hadamard gate condition $\mathcal{C}_1 = \mathcal{C}_2$.

Example 3: Consider a pair of CZ transversal CSS codes $\mathrm{CSS}(\mathcal{C}_1, \mathcal{C}_2)$ and $\mathrm{CSS}(\mathcal{C}_3, \mathcal{C}_4)$, where $\mathrm{CSS}(\mathcal{C}_1, \mathcal{C}_2)$ also has Hadamard transversality, between stations A and B with generator matrices

$$\mathbf{G}_1 = \begin{bmatrix}\mathbf{G}_2^\perp \\ \mathbf{A}\end{bmatrix} = \left[\begin{array}{ccccccc} 0&0&0&1&1&1&1\\ 0&1&1&0&0&1&1\\ 1&0&1&0&1&0&1 \\ \hline 1&1&1&0&0&0&0\end{array}\right].$$

$\mathrm{CSS}(\mathcal{C}_1, \mathcal{C}_2)$ is the Steane code with the transversal Hadamard gate. According to transversal CZ gate conditions (34), we can find the paired code $CSS(\mathcal{C}_3, \mathcal{C}_4)$ as

$$\mathbf{G}_3^\perp = \begin{bmatrix} 0&0&0&1&1&1&1\\ 0&1&1&0&0&1&1\end{bmatrix}$$

and

$$\mathbf{G}_4 = \begin{bmatrix}\mathbf{G}_3^\perp \\ \mathbf{A}\end{bmatrix} = \left[\begin{array}{ccccccc} 0&0&0&1&1&1&1\\ 0&1&1&0&0&1&1\\ \hline 1&1&1&0&0&0&0\end{array}\right].$$

We have $\mathcal{C}_1/\mathcal{C}_2^\perp \cong \mathcal{A}$ and $\mathcal{A} \subset \mathcal{C}_4$. Since $\mathcal{C}_2^\perp \subset \mathcal{C}_3^\perp$, we have $\mathcal{C}_3 \subset \mathcal{C}_2$, which fulfills the condition (34).

In the case of having both CZ and Hadamard gate transversality, one of the two codes used in neighboring stations is a symmetric CSS code, which means that it is not designed for the biased error model (18) governing the 2G QR quantum channel. Thus, for $\mathcal{Q}_{12}$ and $\mathcal{Q}_{34}$ used in stations A and B, choosing $\mathcal{Q}_{12}$ as a symmetric and $\mathcal{Q}_{34}$ as an asymmetric code will lead to worse performance than designing $\mathcal{Q}_{12}$ and $\mathcal{Q}_{34}$ according to the mirrored structure, if the codes have similar minimum distance. The latter construction would, however, necessitate nontransversal Hadamard gates.

There exists a low-cost fault-tolerant manner to realize the logical Hadamard gate for small QECCs [33]. Importantly, this method does not need extra ancilla qubits. As a consequence, we consider mirrored structure CZ-transversal code for 2G QR in the simulations and neglect the cost of local logical Hadamard gates. Keeping only CZ transversality between neighboring stations performs better than also adding a transversal Hadamard restriction on one end.

E. RELATION OF ENCODING AND TRANSVERSALITY

As we showed in the previous sections, the matrices $\mathbf{A}$ and $\mathbf{B}$ introduced in (21) may affect the transversality of the corresponding CSS codes.

It is worth noting that $\mathbf{A}$ and $\mathbf{B}$ define the encoding mapping from logical qubits to physical qubits. Let $\psi_i^A = (0, \ldots, 0, 1, 0, \ldots, 0)$ be the logical state with 1 in the ith position. Then, according to (22), we have

$$|\boldsymbol{\psi}_i^A\rangle = \frac{1}{\sqrt{\mathcal{C}_2^\perp}}\sum_{\mathbf{y}\in\mathcal{C}_2^\perp}|\mathbf{a}_i + \mathbf{y}\rangle.$$

For the same reason, we have

$$|0, 0, \ldots, 0\rangle_L = \frac{1}{\sqrt{\mathcal{C}_2^\perp}}\sum_{\mathbf{y}\in\mathcal{C}_2^\perp}|\mathbf{y}\rangle.$$

If we denote by $\mathbf{X}_L^i \in \mathbb{C}^{2^k}$ the logical Pauli gate that acts by $\mathbf{X}$ on logical qubit i and does not rotate other qubits, then from the above two equations, we have

$$\mathbf{X}_L^i|0,0,\ldots,0\rangle_L = \frac{1}{\sqrt{\mathcal{C}_2^\perp}} \sum_{\mathbf{y}\in\mathcal{C}_2^\perp} |\mathbf{a}_i + \mathbf{y}\rangle. \tag{41}$$

This means that the action of $\mathbf{X}_L^i$ corresponds to adding $\mathbf{a}_i$ to the physical qubits.

From Theorem 1, we know that in order for CSS codes used in stations A and B to be CNOT transversal, it is necessary that $\mathbf{A} = \mathbf{B}$. Combining this with (41), we conclude that for CNOT transversality, it is necessary that realizations of logical $\mathbf{X}$ gates for these codes are identical, despite that the codes themselves are different. Equivalently, the encoding in stations A and B should be the same.

Let us now consider logical CZ transversality. First, we would like to recall that it was shown in [12] and [13] that any self-orthogonal CSS code CSS$(\mathcal{C}, \mathcal{C})$ is CZ transversal. This means that one can use any encoding and still have CZ transversality between any two code vectors. However, from Theorem 1 and Corollary 1, it follows that this is not the case for code vectors from two different CSS codes, which could be used, for example, in stations A and B. Indeed, in this case, the encodings must be such that they guarantee the property $\mathbf{A}\mathbf{B}^T = \mathbf{I}$.

It is worth to note that self-orthogonal CSS codes CSS$(\mathcal{C}, \mathcal{C})$ are a special case of the mirrored structure defined in (36). Thus, our proof of CZ transversality of the mirrored CSS codes gives an alternative proof that self-orthogonal CSS codes are CZ transversal.

To conclude this section, we would like to point out that using the same self-orthogonal CSS code in stations A and B will guarantee CNOT and CZ transversalities despite the choice of encoding operations in stations A and B. It is also efficient for correcting depolarizing errors. However, when the error model is structured, as in the 2G QR system, using a pair of nonidentical CZ-transversal CSS codes specifically designed for the error model will perform better. In Section VI, we shall verify by numerical simulations that using a pair of nonidentical CZ-transversal CSS codes in neighboring stations provides an order of magnitude improvement in the fidelity compared to the case of using the same codes.

F. UNIVERSALITY AND TRANSVERSALITY

In this article, for use in 2G QRs, we study the transversality conditions between different codes, which seems like a potential way to bypass the Eastin–Knill theorem [34]. Here, we will show that it is not possible to achieve universal transversal computation with the {**CNOT** (or **CZ**), **T**, **H**} gate set even when different codes are used to protect different logical bits. Conditions on CSS codes to have a transversal **T** gate have been addressed in the literature [35].

For universal computation with CNOT gates, CNOT gates acting in both directions are needed. Conditions (24) and (25) only guarantee CNOT transversality gate from stations A to B. By doubling the condition for both directions, we find that two CSS codes CSS$(\mathcal{C}_1, \mathcal{C}_2)$ and CSS$(\mathcal{C}_3, \mathcal{C}_4)$ have transversal CNOT gates in both directions only when $\mathcal{C}_1 = \mathcal{C}_3$ and $\mathcal{C}_2 = \mathcal{C}_4$, which means that they are the same code. In such a case, universality and transversality will be limited by the Eastin–Knill theorem.

Now, instead of CNOT gates, consider using the CZ gate to achieve universality. Since the CZ gate does not have control or target qubits, we do not need to consider two directions. Having transversal CZ across two codes, with transversal **T** gate on one end and **H** at the other, is not sufficient for universality; since the CZ gate commutes with the **T** gate, the non-Clifford gates on one side of the CZ gate cannot propagate to another end. Thus, the codes on both ends need to support both transversal **T** and Hadamard gates, which conflicts with the Eastin–Knill theorem.

V. RATE OF QUANTUM COMMUNICATIONS OVER 2G QUANTUM REPEATERS

To quantify the performance of a QR network, we can use two parameters. In addition to logical entanglement fidelity, EGR, indicating the rate of generating end-to-end entangled qubits, is an important factor. These characterize performance irrespectively of whether entanglement is used to generate cryptographic keys or for classical or quantum communication.

Here, we analyze logical EGR for 2G QRs in a system where the overall distance L_T is divided into S hops. The stations are separated with the same nearest neighbor distance $L_0 = L_T/S$. We use M levels for the Bell pair purification protocol, and an $[[n, k]]$ QECC. For the situation of finite-size quantum memory, we use m to indicate the number of qubits in quantum memory.

In the 2G QR system, end-to-end logical entanglement is established in two steps. First, we generate logical entanglement between neighboring stations. Second, by using entanglement swapping, we can achieve overall entanglement. As logical entanglement is generated through the transmission of physical Bell pairs, the EGR of 2G QRs is limited by the speed of generating physical Bell pairs. We define EGR as

$$R = \frac{1}{\tau} \tag{42}$$

where τ is the time it takes to generate one pair of end-to-end entangled logical qubits. It contains three parts

$$\tau = \frac{N_r}{R_{\text{raw}}} + t_{\text{op}} + t_{\text{tr}} \tag{43}$$

where R_{raw} is the raw Bell pair generation rate, N_r is the number of raw Bell pairs consumed to generate one purified pair, t_{op} is the operation time for all local operations, and $t_{\text{tr}} = L_0/c$ is the transmission duration, with c being the speed of light. Assuming that local operations happen in a nanosecond time scale [29], t_{op} is negligible and can be omitted.

IEEE Transactions on Quantum Engineering

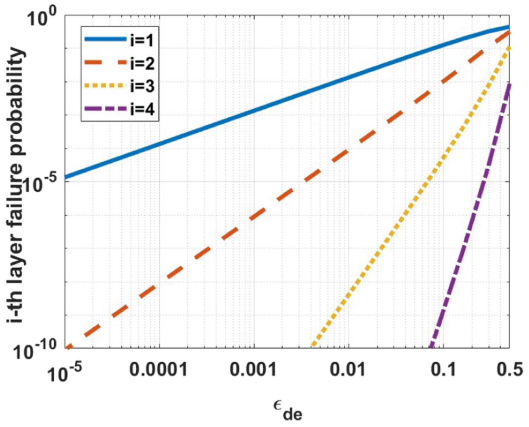

FIGURE 2. Initial depolarizing error rate versus *i*th layer purification failure probability.

There are two processes that consume raw Bell pairs during purification: erasure during transmission, and purification failures. The erasure error rate during transmission is e_0 of (5). The erasure error rate is directly related to the neighboring distance L_0.

Purification success can be summarized as an overall purification success probability p_{tot}. It is related to local operation and physical Bell pair fidelity. In round i of purification, we have success probability p_i of (12). We thus have to consume $2/p_i$ pairs of the previous level for one successfully purified pair on level i. Thus, for one pair on level M, we need to start with $2^M/p_{\text{tot}}$ raw Bell pairs, with $p_{\text{tot}} = \prod_{i=1}^{M} p_s^i$.

Taking erasures into account, for M-level purification, we thus need $2^M/p_{\text{tot}}(1-e_0)$ raw Bell pairs to successfully generate one purified Bell pair. Furthermore, for each logical qubit, we need n/k purified Bell pairs. The number of consumed Bell pairs N_r thus becomes

$$N_r = \frac{2^M n}{(1-e_0)\, p_{\text{tot}}\, k}\,. \tag{44}$$

The relative size of the terms in (43) varies according to the hardware used. In general, if the neighboring distance L_0 is more than 10 km, the qubit generation time cost N_r/R_{raw} is much smaller than the transmission duration t_{tr} [29].

To model errors in Bell pair purification, we assume that the raw Bell pairs suffer from depolarizing errors, such that $f_1 = f_2 = f_3 = \varepsilon_{de}/3$. The purification success probabilities (12) can then be solved from the recursion (11). In Fig. 2, we have plotted p_s^i as a function of ε_{de} for $i = 1, \ldots, 4$. For all values $\varepsilon_{de} < 0.5$, the second level purification failure probability is much smaller than the first level; $(1-p_s^i) \ll (1-p_s^1)$. Thus, we can ignore the purification success failures for levels $i > 1$, and assume $p_{\text{tot}} \approx p_1$.

The time consumption of the transmission procedure depends on the size of the quantum memory. With unlimited quantum memory, an unlimited number of Bell pairs can be transmitted, and all the qubits needed for purification can be stored in quantum memory to wait for further operations. Thus, the procedure suffers from the delay only in the setup phase from the first transmission and the following classical communication for purification measurement. Under these circumstances, only the distance between neighboring stations L_0 would affect the transmission time cost.

The situation changes if there is limited quantum memory. In order to finish purification, several rounds of transmission are needed. The transmission time depends on the required number of Bell pairs N_r and will grow along with the selected purification level M and purification success probability p_s. The time cost of transmission procedure comes from the following steps.

1) The transmitter sends m photonic qubits through the fiber to the receiver. We assume that m is smaller than the number N_r of required qubits from (44).
2) The receiver uses heralded entanglement generation to correct erasure errors with the help of classical communication. The delay of this procedure is taken into account in the e_0-dependence of N_r.
3) The transmitter sends additional qubits to fill up the quantum memory. On average, $\frac{N_r}{m}$ rounds of transmission will be needed. For each round, there are two communication events: first the qubit transmissions and then the classical feedback. The average time cost is thus $2\frac{N_r}{m}\frac{L_0}{c}$.

From this, we get the EGR for a limited quantum memory situation

$$\tau = \frac{N_r}{m}\left(\frac{m}{R_{\text{raw}}} + 2\frac{L_0}{c}\right) + M\frac{L_0}{c}. \tag{45}$$

Here, the factor 2 in the second term in the parenthesis indicates two-way quantum and classical communication with heralded entanglement generation. The last term is contributed by classical commination in the M-level purification procedure.

In a practical scenario, we consider a system built for generating end-to-end entanglement between two stations far apart. The quantum communication service requirements are expressed in terms of an EGR and overall logical fidelity thresholds. The overall logical fidelity can be expressed as

$$f_T = f_L^{2S} \tag{46}$$

where f_L is logical fidelity in each code block and S is the number of hops. The logical fidelity f_L is a function of the neighboring distance L_0, purification level M, and local gate error rate f_g. The cost of building the system is computed as the number of needed intermediate stations. To minimize cost, the neighboring distance L_0 should be maximized. This leads to the optimization problem

$$\begin{aligned} &\max L_0 \\ \text{s.t.}\quad &R(L_0, M) \geq R_{\text{th}} \\ &f_T\left(L_0, M, f_g\right) \geq f_{\text{th}}\,. \end{aligned}$$

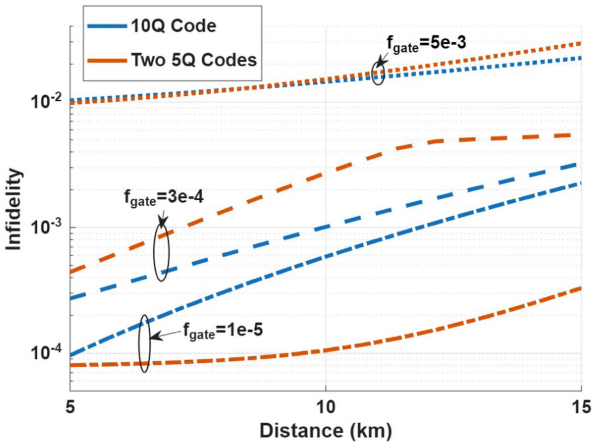

FIGURE 3. Performance in the correlated error channel (18). Crossover behavior between symmetric (ten-qubit) and nonsymmetric (two five-qubit) codes with same minimum distance. The infidelity as a function of distance between neighboring stations for different two-qubit gate error rates.

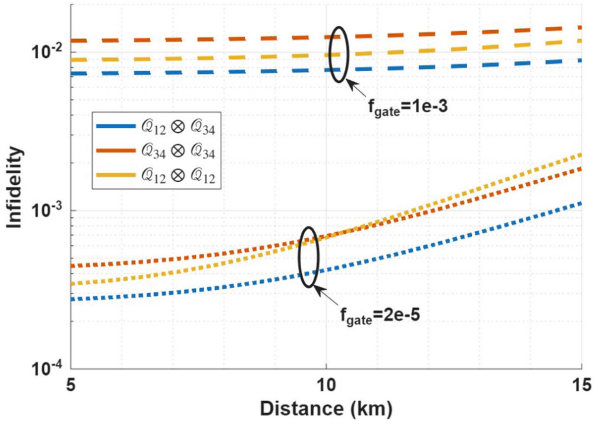

FIGURE 4. Infidelity as a function of distance between neighboring stations with CNOT transversal structure, for different two-qubit gate error rates. Codes from Example 1.

Here, R_{th} and f_{th} are desired thresholds for EGR and the overall logical fidelity for reliable quantum communication. With fixed overall distance L_T, by maximizing L_0, we get the minimum number of intermediate stations. We shall consider this optimization numerically in the next section.

VI. NUMERICAL RESULTS

In this section, we provide numerical results to evaluate the infidelity and EGR in QRs. We use the distance-dependent error model (7) with $\alpha = 0.17$ dB/km and $\beta = 0.01$ /km. With neighboring distance L_0, the raw Bell pairs (9) after transmission have $f_1 = f_2 = f_3 = (1 - e^{-0.01L_0})/3$ [36] as initial values of the recursion (11). For infidelity simulation, we consider different levels M of purification and use the maximum likelihood decoder [37]. For numerical EGR results, we set the photonic qubit generation rate as $R_{\text{raw}} = 10^6$ [29]. We neglect photonic qubit detection errors and quantum memory decoherence. For limited quantum memory situation, we assume that each station has $m = 100$ memory qubits for storing information.

First, following Section III-E, we compare symmetric and nonsymmetric codes with the same minimum distance, which means that they have similar performance for depolarizing errors. We study their infidelity performance under the correlated error model (18). In Fig. 3, we compare the performance of two alternatives: one is using a symmetric $[[10, 2, 3]]$ CSS code to protect two logical qubits at each station, and the other is using two five-qubit nonsymmetric codes in parallel as $[[5, 1, 3]]^{\otimes 2}$ codes to protect the two logical qubits, in channel (18). Note that, here, the same code is used at both stations A and B, and joint decoding is performed between neighboring stations using a maximum-likelihood algorithm. The purification level is $M = 4$. The infidelity of the logical qubits is plotted against gate error probability and distance.

In the large neighboring distance area, where the correlated errors are dominant, the nonsymmetric codes achieve better performance. This is due to the fact that the nonsymmetric codes are designed to handle correlated **ZX** errors. This is concordance with Proposition 1, which states that a nonsymmetric CSS code outperforms a symmetric code under the correlated error scenario. When depolarizing gate errors dominate, these two codes have similar performance since they have the same minimum distance.

Next, following Section IV, we consider using pairs of different codes at neighboring stations under error model (16) and purification level $M = 4$. We compare the performance of pairs of codes, which are CNOT or CZ transversal with the case of using the same CSS code at neighboring stations. In this case, joint decoding is unnecessary and maximum-likelihood decoding is used separately at each station instead.

Fig. 4 compares the infidelity with the CNOT transversal structures. In this figure, $\mathcal{Q}_{12} = \text{CSS}(\mathcal{C}_1, \mathcal{C}_2)$ and $\mathcal{Q}_{34} = \text{CSS}(\mathcal{C}_3, \mathcal{C}_4)$ are CSS codes $[[7, 1, 2]]$ based on Example 1. Note that the minimum distances of $\mathcal{Q}_{12}$ and $\mathcal{Q}_{34}$ are $d = 2$. In this figure, $\mathcal{Q}_{12} \otimes \mathcal{Q}_{34}$ means that stations A and B are using $\mathcal{Q}_{12}$ and $\mathcal{Q}_{34}$, respectively. $\mathcal{Q}_{12}$ and $\mathcal{Q}_{34}$ are designed to satisfy the CNOT transversality condition. It is seen that the use of the $\mathcal{Q}_{12} \otimes \mathcal{Q}_{34}$ CSS structure results in better performance in comparison to using the same code at the stations.

In Fig. 5, we also compare the logical infidelity between the [[7,1,3]] symmetric Steane code and the [[7,1,2]] mirrored structure nonsymmetric code, which consists of $\mathcal{C}_1(7, 2, 4)$ with the generator matrix

$$\mathbf{G}_1 = \begin{bmatrix} 1 & 0 & 0 & 1 & 1 & 0 & 0 \\ 0 & 1 & 1 & 0 & 0 & 1 & 1 \end{bmatrix}$$

and $\mathcal{C}_2(7, 6, 2)$ with the parity check matrix

$$\mathbf{G}_2^{\perp} = \begin{bmatrix} 1 & 1 & 1 & 1 & 1 & 1 & 1 \end{bmatrix}$$

IEEE Transactions on Quantum Engineering

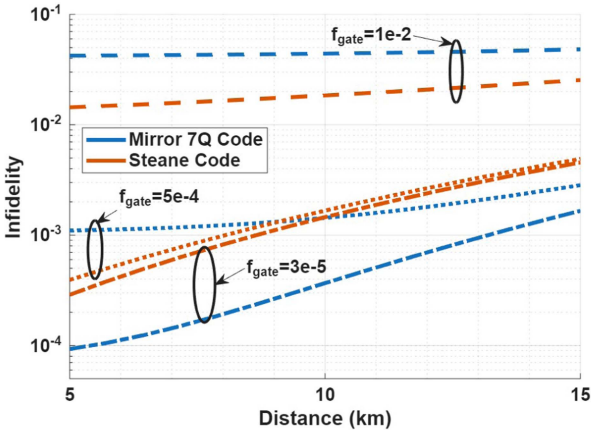

FIGURE 5. Comparison between the [[7,1,3]] Steane code (CNOT transversal) and the [[7,1,2]] nonsymmetric code with a mirrored structure (CZ transversal).

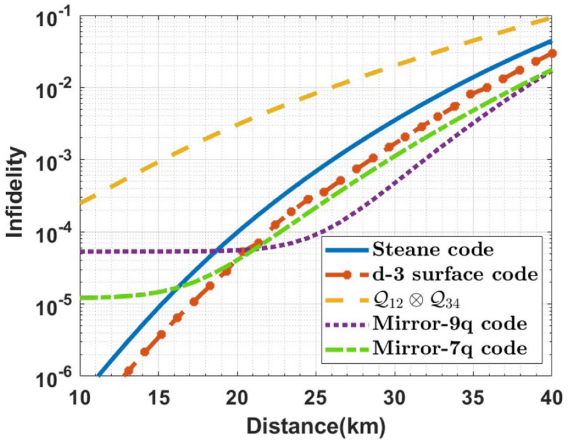

FIGURE 7. Relation between the infidelity of different codes and the neighboring station distance. The local gate error rate is set to 10^{-5}.

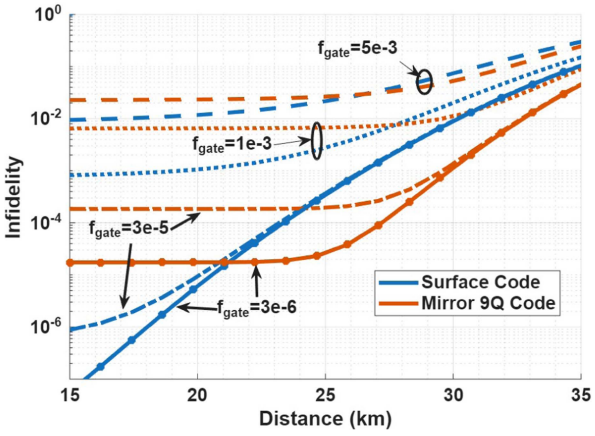

FIGURE 6. Comparison between the [[9,1,3]] distance-3 surface code (CNOT transversal) and the [[9,1,2]] nonsymmetric code with a mirrored structure (CZ transversal).

at station A and has five Pauli-X stabilizers and one Pauli-Z generators. In station B, we use code CSS($\mathcal{C}_2, \mathcal{C}_1$). When the biased error is significant, i.e., when the neighboring distance L_0 is relatively large, the mirrored structure outperforms the surface code, despite its smaller minimum distance.

In Fig. 6, we compare the performance of the mirrored approach with the case of using similar symmetric CSS codes in both stations of a QR system. We consider purification level $M = 6$. For a mirrored structure, in station A, $\mathcal{C}_1(9, 2, 5)$ with the generator

$$\mathbf{G}_1 = \begin{bmatrix} 1 & 1 & 1 & 1 & 0 & 0 & 0 & 0 & 0 \\ 0 & 0 & 0 & 0 & 1 & 1 & 1 & 1 & 1 \end{bmatrix}$$

and $\mathcal{C}_2$ $(9, 8, 2)$ with the parity check matrix

$$\mathbf{G}_2^{\perp} = \begin{bmatrix} 1 & 1 & 1 & 1 & 1 & 1 & 1 & 1 & 1 \end{bmatrix}$$

are used to construct a nonsymmetric [[9,1,2]] CSS code, which has seven Pauli-X stabilizers and one Pauli-Z generators. In station B, we use code CSS($\mathcal{C}_3, \mathcal{C}_4$) where $\mathcal{C}_3 = \mathcal{C}_2$ and $\mathcal{C}_4 = \mathcal{C}_1$. As a result, this quantum code has one Pauli-X stabilizer and seven Pauli-Z generators. With the mirrored approach, we have CZ transversality in neighboring stations. This is benchmarked against the [[9, 1, 3]] surface code, which is symmetric, has CNOT transversality, and has distance-3.

In Fig. 7, we compare the infidelity of several codes: Steane code, distance-3 surface code, CNOT transversal codes $\mathcal{Q}_{12} \otimes \mathcal{Q}_{34}$, and the mirrored structure nine- and seven-qubit codes. The gate error rate is set to 10^{-5}. In the regime of large neighboring distances, where the biased errors dominate, the mirrored structure codes have lower infidelity than others, as they are specifically designed to handle such errors. The nine-qubit mirrored code outperforms the seven-qubit code in the mid-distance range (from 20 to 35 km). However, as the distance increases further, biased errors accumulate significantly across the larger code block, such that the infidelity of the nine-qubit mirrored code approaches the seven-qubit one. In such cases, achieving better performance with larger codes would require increasing the purification level to better suppress biased errors. At lower distances, where gate errors dominate, conventional codes outperform the mirrored structure due to their larger code distance. In this regime, the seven-qubit mirrored code achieves higher fidelity than the nine-qubit version, as it involves fewer gate operations. It is also worth noting that the CNOT transversal code always has the highest infidelity among all codes considered, due to its lower code distance and not designed for protecting against biased errors.

Next, we analyze the effect of the code structure and channel parameters on communication performance. First, in Fig. 8, we show the relation between EGR and the overall distance for different numbers of intermediate stations with nine-qubit codes used in Fig. 6. Note that using the same

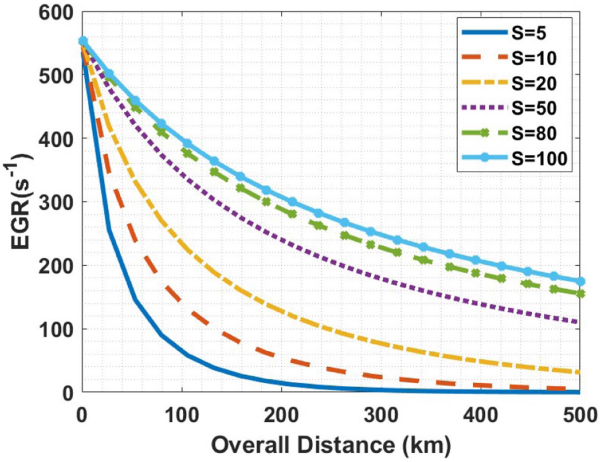

FIGURE 8. Relation between EGR and overall distance, for different numbers S of intermediate stations. We choose nine-qubit mirrored structure code and set the purification level $M = 6$ and local operation error $f_g = 10^{-5}$.

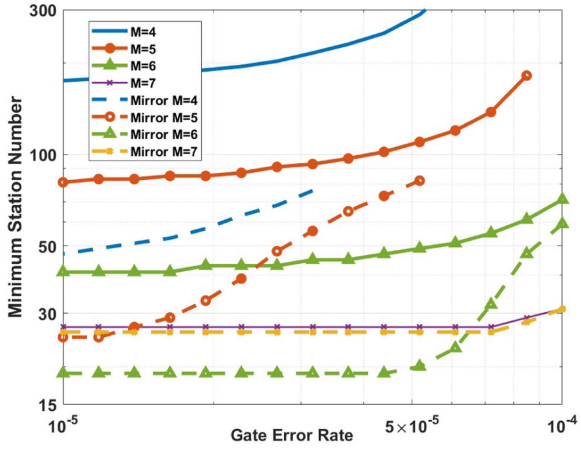

FIGURE 9. Minimum intermediate station number versus local gate error rate, for overall distance 500 km, EGR $R_{\text{th}} = 50$ entangled qubits/s, and overall logical fidelity threshold $f_{\text{th}} = 0.95$. The parameter M denotes the purification level of the Bell states. The Steane code is compared to the mirrored CSS seven-qubit code with purification level $M = 4, 5, 6, 7$.

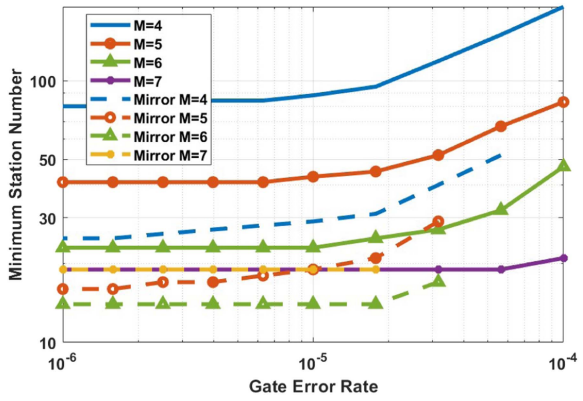

FIGURE 10. Minimum intermediate station number versus local gate error rate for overall distance 500 km. The distance-3 surface code is compared to the mirrored CSS nine-qubit code with same parameter as in Fig. 9. The parameter M denotes the purification level of the Bell states.

distance-3 surface code or the mirrored structure nonsymmetric codes does not affect the EGR of (45); it only affects the infidelity. When the overall distance is small, the EGR approaches an upper bound given by the photonic qubit generation rate.

In Fig. 9, we compare the minimum number of intermediate stations when using seven-qubit mirrored structure [[7,1,2]] code and the [[7,1,3]] Steane code, as in Fig. 5, given EGR and fidelity threshold requirements $R_{\text{th}} = 50$ qubit/s and $f_{\text{th}} = 0.95$. When the gate error approaches 10^{-5}, the distance-related errors dominate, and fulfilling the logical fidelity threshold becomes independent of the local gate error rate. For purification levels $M = 4, 5, 6$, using mirrored structure codes can reduce the number of stations significantly. This is because the mirrored structure codes can correct more distance-related errors and, thus, have much higher logical fidelity. However, for $M = 4, 5$ and a large gate error rate, we cannot find a station number for the mirrored structure that meets all the thresholds. When we set $M = 7$, using both codes can have high logical fidelity above the fidelity threshold. In this situation, the minimum station number is limited by the EGR. Since both codes use the same number of qubits, their EGRs are the same. Thus, with larger purification level, codes have higher fidelity, but the EGR is limited by the larger resource cost. Overall, in this tradeoff, the smallest number of stations is provided by $M = 6$ and the mirrored structure for gate error rate $< 5 \times 10^{-5}$.

Finally, in Fig. 10, we compare between larger codes, the nine-qubit mirrored structure codes, and distance-3 surface code, as in Fig. 6, with the same parameters as in Fig. 9. Compared with seven-qubit codes, we can see that nine-qubit codes need less intermediate stations in the low gate error rate region. The nine-qubit code reach its best performance when $M = 6$, but the minimum station number gap between $M = 5$ and the optimal case is smaller than for seven-qubit codes. In low gate error case, setting $M = 5$ provides near-optimum performance while reducing the consumption of Bell pair resources. This also indicates that a larger code can reach optimal performance with a lower purification level than a smaller code.

VII. CONCLUSION

In this article, we have investigated a distance-related error model for 2G QRs, which has both correlated and biased errors. Based on this error model, we showed that nonsymmetric CSS codes outperform symmetric ones for 2G QRs. To improve the error correction performance, we proposed to use different codes at the neighboring stations and introduced the class of code pairs with a mirrored structure. Nonsymmetric codes target correlated errors, while the mirrored structure works against biased errors. We studied the

transversality of the nonlocal CNOT gates essential for 2G QRs in a situation with two different CSS codes used for error correction at neighboring stations. We found less restrictive constraints in this case than when using the same CSS code in the neighboring stations. Also, we found sufficient conditions for having a nonlocal transversal CZ gate between the neighboring stations. Finally, we computed the rate of creating end-to-end entanglement in 2G QR system with limited quantum memory. Based on this, we numerically minimized the number of intermediate stations for achieving reliable end-to-end quantum communication with a given overall distance and gate error rate.

REFERENCES

[1] L. Jiang, J. M. Taylor, K. Nemoto, W. J. Munro, R. Van Meter, and M. D. Lukin, "Quantum repeater with encoding," *Phys. Rev. A*, vol. 79, no. 3, 2009, Art. no. 032325, doi: 10.1103/PhysRevA.79.032325.

[2] W. K. Wootters and W. H. Zurek, "A single quantum cannot be cloned," *Nature*, vol. 299, pp. 802–803, 1982, doi: 10.1038/299802a0.

[3] D. Gottesman, T. Jennewein, and S. Croke, "Longer-baseline telescopes using quantum repeaters," *Phys. Rev. Lett.*, vol. 109, no. 7, 2012, Art. no. 070503, doi: 10.1103/PhysRevLett.109.070503.

[4] C. Simon, "Towards a global quantum network," *Nat. Photon.*, vol. 11, no. 11, pp. 678–680, 2017, doi: 10.1038/s41566-017-0032-0.

[5] W. Kozlowski and S. Wehner, "Towards large-scale quantum networks," in *Proc. ACM Int. Conf. Nanoscale Comput. Commun.*, 2019, pp. 1–7, doi: 10.1145/3345312.3345497.

[6] H.-J. Briegel, W. Dür, J. I. Cirac, and P. Zoller, "Quantum repeaters: The role of imperfect local operations in quantum communication," *Phys. Rev. Lett.*, vol. 81, no. 26, 1998, Art. no. 5932, doi: 10.1103/PhysRevLett.81.5932.

[7] L. Childress, J. Taylor, A. S. Sørensen, and M. Lukin, "Fault-tolerant quantum communication based on solid-state photon emitters," *Phys. Rev. Lett.*, vol. 96, no. 7, 2006, Art. no. 070504, doi: 10.1103/PhysRevLett.96.070504.

[8] W. Dür, H.-J. Briegel, J. I. Cirac, and P. Zoller, "Quantum repeaters based on entanglement purification," *Phys. Rev. A*, vol. 59, no. 1, 1999, Art. no. 169, doi: 10.1103/PhysRevA.59.169.

[9] N. Sangouard, C. Simon, H. De Riedmatten, and N. Gisin, "Quantum repeaters based on atomic ensembles and linear optics," *Rev. Modern Phys.*, vol. 83, no. 1, 2011, Art. no. 33, doi: 10.1103/RevModPhys.83.33.

[10] S. Muralidharan, J. Kim, N. Lütkenhaus, M. D. Lukin, and L. Jiang, "Ultrafast and fault-tolerant quantum communication across long distances," *Phys. Rev. Lett.*, vol. 112, no. 25, 2014, Art. no. 250501, doi: 10.1103/PhysRevLett.112.250501.

[11] M. A. Nielsen and I. L. Chuang, *Quantum Computation and Quantum Information*. Cambridge, U.K.: Cambridge Univ. Press, 2000, doi: 10.1017/CBO9780511976667.

[12] S. Muralidharan, L. Li, J. Kim, N. Lütkenhaus, M. D. Lukin, and L. Jiang, "Optimal architectures for long distance quantum communication," *Sci. Rep.*, vol. 6, no. 1, 2016, Art. no. 20463, doi: 10.1038/srep20463.

[13] P. van Loock et al., "Extending quantum links: Modules for fiber- and memory-based quantum repeaters," *Adv. Quantum Technol.*, vol. 3, no. 11, 2020, Art. no. 1900141, doi: 10.1002/qute.201900141.

[14] L. Valentini, R. B. Christensen, P. Popovski, and M. Chiani, "Reliable quantum communications based on asymmetry in distillation and coding," *IEEE Trans. Quantum Eng.*, vol. 5, 2024, Art. no. 4100613, doi: 10.1109/TQE.2024.3399609.

[15] Q. Xu et al., "Fast and parallelizable logical computation with homological product codes," *Phys. Rev. X*, vol. 15, no. 2, May 22, 2025, Art. no. 021065, doi: 10.1103/PhysRevX.15.021065.

[16] D. Horsman, A. G. Fowler, S. Devitt, and R. V. Meter, "Surface code quantum computing by lattice surgery," *New J. Phys.*, vol. 14, no. 12, Dec. 2012, Art. no. 123011, doi: 10.1088/1367-2630/14/12/123011.

[17] S. Bravyi, G. Smith, and J. A. Smolin, "Trading classical and quantum computational resources," *Phys. Rev. X*, vol. 6, no. 2, 2016, Art. no. 021043, doi: 10.1103/PhysRevX.6.021043.

[18] F. Butt, S. Heußen, M. Rispler, and M. Müller, "Fault-tolerant code-switching protocols for near-term quantum processors," *PRX Quantum*, vol. 5, no. 2, May 2024, Art. no. 020345, doi: 10.1103/PRXQuantum.5.020345.

[19] W. Brown and O. Fawzi, "Short random circuits define good quantum error correcting codes," in *Proc. IEEE Int. Symp. Inf. Theory*, 2013, pp. 346–350, doi: 10.1109/ISIT.2013.6620245.

[20] B. M. Terhal, M. Horodecki, D. W. Leung, and D. P. DiVincenzo, "The entanglement of purification," *J. Math. Phys.*, vol. 43, no. 9, pp. 4286–4298, 2002, doi: 10.1063/1.1498001.

[21] S. Bose, V. Vedral, and P. L. Knight, "Multiparticle generalization of entanglement swapping," *Phys. Rev. A*, vol. 57, no. 2, 1998, Art. no. 822, doi: 10.1103/PhysRevA.57.822.

[22] D. Gottesman, "Opportunities and challenges in fault-tolerant quantum computation," 2022, *arXiv:2210.15844*, doi: 10.48550/arXiv.2210.15844.

[23] D. Gottesman, "Stabilizer codes and quantum error correction," M.S. thesis, Division Phys., Math. Astron., California Inst. Technol., Pasadena, CA, USA, 1997, doi: 10.48550/arXiv.quant-ph/9705052.

[24] A. R. Calderbank and P. W. Shor, "Good quantum error-correcting codes exist," *Phys. Rev. A*, vol. 54, no. 2, 1996, Art. no. 1098, doi: 10.1103/PhysRevA.54.1098.

[25] P. W. Shor, "Fault-tolerant quantum computation," in *Proc. Conf. Found. Comput. Sci.*, 1996, pp. 56–65, doi: 10.1109/SFCS.1996.548464.

[26] D. Deutsch, A. Ekert, R. Jozsa, C. Macchiavello, S. Popescu, and A. Sanpera, "Quantum privacy amplification and the security of quantum cryptography over noisy channels," *Phys. Rev. Lett.*, vol. 77, no. 13, 1996, Art. no. 2818, doi: 10.1103/PhysRevLett.77.2818.

[27] X. Zhou, D. W. Leung, and I. L. Chuang, "Methodology for quantum logic gate construction," *Phys. Rev. A*, vol. 62, no. 5, 2000, Art. no. 052316, doi: 10.1103/PhysRevA.62.052316.

[28] S. Muralidharan, C.-L. Zou, L. Li, J. Wen, and L. Jiang, "Overcoming erasure errors with multilevel systems," *New J. Phys.*, vol. 19, no. 1, 2017, Art. no. 013026, doi: 10.1088/1367-2630/aa573a.

[29] R. Valivarthi et al., "Efficient bell state analyzer for time-bin qubits with fast-recovery WSI superconducting single photon detectors," *Opt. Exp.*, vol. 22, no. 20, pp. 24497–24506, 2014, doi: 10.1364/OE.22.024497.

[30] Google Quantum AI, "Suppressing quantum errors by scaling a surface code logical qubit," *Nature*, vol. 614, no. 7949, pp. 676–681, 2023, doi: 10.1038/s41586-022-05434-1.

[31] D. Jiao, A. Ashikhmin, M. Bayanifar, and O. Tirkkonen, "Using small dimensional quantum error correction codes for high-performance quantum communication," in *Proc. IEEE Glob. Commun. Conf.*, 2023, pp. 1387–1392, doi: 10.1109/GLOBECOM54140.2023.10436732.

[32] M. Bayanifar, A. Ashikhmin, D. Jiao, and O. Tirkkonen, "Transversality across two distinct quantum codes and its application to quantum repeaters," in *Proc. IEEE Internat Conf. Quantum Commun., Netw., Comput.*, 2025, pp. 17–23, doi: 10.1109/QCNC64685.2025.00013.

[33] T. J. Yoder, R. Takagi, and I. L. Chuang, "Universal fault-tolerant gates on concatenated stabilizer codes," *Phys. Rev. X*, vol. 6, no. 3, 2016, Art. no. 031039, doi: 10.1103/PhysRevX.6.031039.

[34] B. Eastin and E. Knill, "Restrictions on transversal encoded quantum gate sets," *Phys. Rev. Lett.*, vol. 102, no. 11, 2009, Art. no. 110502, doi: 10.1103/PhysRevLett.102.110502.

[35] N. Rengaswamy, R. Calderbank, M. Newman, and H. D. Pfister, "On optimality of CSS codes for transversal T," *IEEE J. Sel. Areas Inf. Theory*, vol. 1, no. 2, pp. 499–514, Aug. 2020, doi: 10.1109/JSAIT.2020.3012914.

[36] Z.-H. Xiang et al., "Long-term transmission of entangled photons from a single quantum dot over deployed fiber," *Sci. Rep.*, vol. 9, no. 1, 2019, Art. no. 4111, doi: 10.1038/s41598-019-40912-z.

[37] G. D. Forney Jr., "Convolutional codes II. Maximum-likelihood decoding," *Inf. Control*, vol. 25, no. 3, pp. 222–266, 1974, doi: 10.1016/S0019-9958(74)90870-5.